7-1-2009

Srs2 Disassembles Rad51 Filaments by a Protein-Protein Interaction Triggering ATP Turnover and Dissociation of Rad51 from DNA

Edwin Antony
Marquette University, edwin.antony@marquette.edu

Eric J. Tomko
Washington University School of Medicine in St. Louis

Qi Xiao
Washington University in St Louis

Lumir Krejci
Masaryk University

Timothy M. Lohman
Washington University School of Medicine in St. Louis

See next page for additional authors

Accepted version. *Molecular Cell*, Vol. 35, No. 1 (July 2009): 105-115. DOI.
Edwin Antony was affiliated with Washington University at time of publication.

Srs2 Disassembles Rad51 Filaments by a Protein-Protein Interaction Triggering ATP Turnover and Dissociation of Rad51 from DNA

Edwin Antony
Department of Biochemistry and Molecular Biophysics, Washington University School of Medicine
St. Louis, MO
Eric J. Tomko
Department of Biochemistry and Molecular Biophysics, Washington University School of Medicine
St. Louis, MO
Qi Xiao
Young Scientist Program, Washington University in St. Louis
St. Louis, MO
Lumir Krejci
National Centre for Biomolecular Research and Department of Biology, Masaryk University
Brno, Czech Republic

Molecular Cell, Vol. 35, No. 1 (July 10, 2009): pg. 105-115. DOI.

Timothy M. Lohman
Department of Biochemistry and Molecular Biophysics,
Washington University School of Medicine
St. Louis, MO
Tom Ellenberger
Department of Biochemistry and Molecular Biophysics,
Washington University School of Medicine
St. Louis, MO

Summary

Rad51 is a DNA recombinase functioning in the repair of DNA double-strand breaks and the generation of genetic diversity by homologous recombination (HR). In the presence of ATP, Rad51 self-assembles into an extended polymer on single-stranded DNA to catalyze strand exchange. Inappropriate HR causes genomic instability and it is normally prevented by remodeling enzymes that antagonize the activities of Rad51 nucleoprotein filaments. In yeast, the Srs2 helicase/translocase suppresses HR by clearing Rad51 polymers from single-stranded DNA. We have examined the mechanism of disassembly of Rad51 nucleoprotein filaments by Srs2 and find that a physical interaction between Rad51 and the C-terminal region of Srs2 triggers ATP hydrolysis within the Rad51 filament, causing Rad51 to dissociate from DNA. This allosteric mechanism explains the biological specialization of Srs2 as a DNA motor protein that antagonizes HR.

Introduction

Homologous recombination (HR) is an important mechanism for the repair of DNA double-stranded breaks (DSBs), which arise normally during meiosis or as a result of exposure to DNA damaging agents (Li and Heyer, 2008). In eukaryotes, the ATP-dependent recombinase Rad51 catalyzes DNA strand exchange during HR in conjunction with pro- and anti-recombinogenic regulatory proteins that assist or inhibit Rad51's interactions with DNA substrates (Bianco et al., 1998). Rad51 is a member of the RecA family of recombinases, which assemble into a right-handed helical filament on single-stranded DNA (ssDNA) that activates downstream steps of HR (Sung and Klein,

Molecular Cell, Vol. 35, No. 1 (July 10, 2009): pg. 105-115. DOI.

2006). Inherited defects in HR predispose cells to genomic instability and disease. For example, the breast cancer-associated tumor suppressor BRCA2 physically interacts with the Rad51 recombinase to regulate the assembly and stability of the Rad51 nucleoprotein filament (Pellegrini and Venkitaraman, 2004; Thorslund and West, 2007). Mutations in BRCA2 that compromise these functions are associated with an increased incidence of chromosomal rearrangements and other aberrations.

In the budding yeast *Saccharomyces cerevisiae*, HR is coordinated by proteins of the *RAD52* epistasis group that function as positive mediators of Rad51 functions, conferring normal cellular resistance to DNA strand breaks and other types of damage (Li and Heyer, 2008; Sung and Klein, 2006; Symington, 2002). DNA DSBs are nucleolytically resected to generate a 3′ single-stranded tail of about 600 nt that serves as a template for the assembly of a pre-synaptic Rad51 filament. The Rad51 filament invades an undamaged double-stranded DNA (dsDNA) where homologous sequences can pair in a synaptic complex. Once homology is identified, the dsDNA is used as a template to extend the invading strand by DNA synthesis. This newly synthesized strand is then resolved into a continuous double-stranded DNA product by one of several pathways leading to crossovers and noncrossover products (Bianco et al., 1998; Krogh and Symington, 2004).

The nucleation of Rad51 filament growth on ssDNA provides a window of opportunity for the regulation of HR activity by both pro- and anti-recombinogenic factors. *Saccharomyces cerevisiae* Srs2 is a negative regulator of HR that disrupts preformed Rad51 filaments (Krejci et al., 2003; Veaute et al., 2003), and a similar activity has been recently ascribed to two mammalian RecQ-type helicases (Bugreev et al., 2007; Hu et al., 2007). The anti-recombinogenic activity of Srs2, which is attributed to the disassembly of Rad51 filaments is regulated by the recruitment of Srs2 to sites of DNA damage following checkpoint activation, possibly through phosphorylation of Srs2 by CDK-1 (Chiolo et al., 2005) and/or through the physical interaction with sumoylated PCNA (Papouli et al., 2005; Pfander et al., 2005). Srs2 physically interacts with Rad51, although the functional significance of this interaction for Srs2's anti-

Molecular Cell, Vol. 35, No. 1 (July 10, 2009): pg. 105-115. DOI.

recombinogenic activities has not been established (Krejci et al., 2003).

Srs2 belongs to the SF-1 superfamily of helicases/translocases and possesses a DNA unwinding activity coupled to ATP hydrolysis (Rong and Klein, 1993). These activities have been well characterized in other SF-1 family members (Lohman et al., 2008; Singleton et al., 2007). Monomers of the SF-1 enzymes Rep, PcrA, and UvrD are rapid, processive translocases on ssDNA; however, DNA unwinding activity requires oligomerization *in vitro* (Lohman et al., 2008). Hence, for these enzymes, DNA unwinding and ssDNA translocation activities are separable. The conserved SF-1 family motifs of Srs2 define a core architecture that is likely to closely resemble the structures of the SF-1 helicases UvrD (Lee and Yang, 2006), PcrA (Velankar et al., 1999), and Rep (Korolev et al., 1997). However, Srs2 has an additional 454 amino acids at its C-terminus (Figure 1) that mediate interactions with Rad51 (Krejci et al., 2003) and PCNA (Papouli et al., 2005; Pfander et al., 2005), and may confer specificity to the remodeling of nucleoprotein filaments. UvrD, a bacterial homolog of Srs2, similarly antagonizes the formation of RecA filaments in bacteria (Veaute et al., 2005).

Molecular Cell, Vol. 35, No. 1 (July 10, 2009): pg. 105-115. DOI.

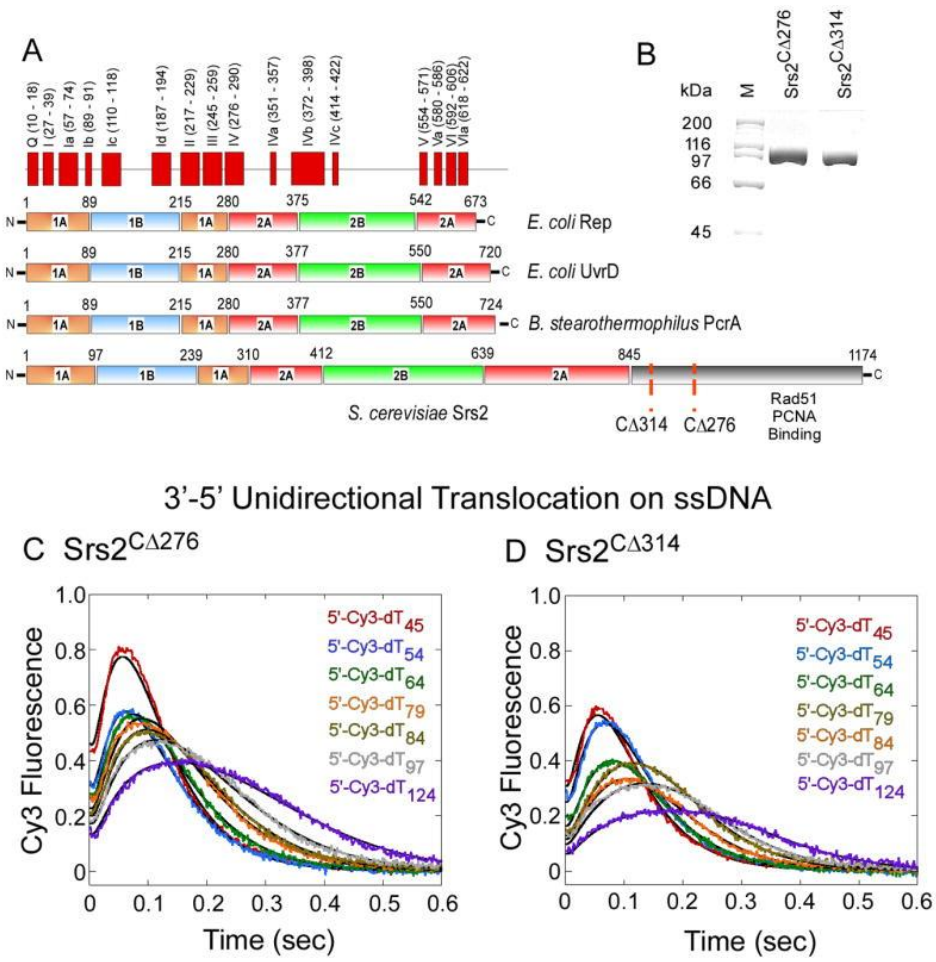

Figure 1: Srs2 Translocates Unidirectionally on ssDNA
(A) Sequence alignment of *Saccharomyces cerevisiae* Srs2 with various bacterial SF-1 helicases. The conserved helicase motifs, 1A, 2A, 1B and 2B domains in UvrD are depicted. (B) SDS-PAGE analysis of the purified Srs2 proteins used in this study: $Srs2^{C\Delta276}$ and $Srs2^{C\Delta314}$. (C, D) Time courses monitoring Cy3 fluorescence on 5'Cy3 labeled oligonucleotides of varying lengths (25 – 124 nt) shows that $Srs2^{C\Delta276}$ and $Srs2^{C\Delta314}$ translocate unidirectionally on ssDNA.

Using real-time assays, we have monitored the dynamics of the Rad51 filament and its disassembly by Srs2. We identify features of Srs2-mediated clearing of Rad51 nucleoprotein filaments that distinguish this specialized activity from DNA translocation and unwinding activities. Our findings show that the unidirectional translocation of Srs2 on ssDNA does not by itself account for the enzymatic clearance of Rad51 filaments. Instead, the physical interaction of Srs2 with the Rad51 protein allosterically activates ATP hydrolysis within the Rad51 nucleoprotein filament to promote clearing of Rad51 from the DNA. Although the bacterial UvrD helicase can

displace yeast Rad51 from DNA (Veaute et al., 2005), we show that this activity is noncatalytic and results from a binding competition with Rad51 for DNA. The anti-recombinogenic activity of Srs2 results from a protein-protein interaction that imparts biological specificity to its DNA remodeling functions.

Results

Srs2 Unidirectionally Translocates on ssDNA

To obtain large quantities of Srs2 and alleviate the problem of protein aggregation, we deleted portions of the nonconserved C-terminal region and found that fragments spanning amino acids 1-860 ($Srs2^{C\Delta314}$ and 1-898 ($Srs2^{C\Delta276}$; Figure 1A) are well behaved proteins that elute from a gel filtration column as a single peak with the expected apparent molecular size for a monomer (Figures 1B & S1). Both truncated proteins exhibit similar DNA unwinding activities (data not shown), whereas the Rad51-specific functions of Srs2 are eliminated in the shorter $Srs2^{C\Delta314}$ construct, as shown below.

SF-1 helicases translocate with biased directionally along ssDNA in an ATP-dependent manner (Lohman et al., 2008). DNA translocation by Srs2 could assist in remodeling Rad51 nucleoprotein filaments. Translocation activity was measured on a series of single-stranded dT_n oligonucleotides of different lengths (5′-Cy3-dT_n; n = 45 - 124 nucleotides, Figures 1C & D) using a single turnover assay (Fischer et al., 2004; Tomko et al., 2007). The arrival of Srs2 at the 5′ end of DNA labeled with Cy3 is accompanied by an increase in Cy3 fluorescence intensity. With increasing length (n) of the DNA, the distribution of fluorescence events broadens and the average time required for Srs2 to arrive at the 5′ end increases, reflecting random binding of Srs2 to the DNA and movement in a 3′ to 5′ direction (Figure 1C & 1D). Similar experiments with the Cy3 label on the 3′ end of the DNA did not produce a change in fluorescence intensity, consistent with the unidirectional translocation of Srs2 towards the 5′ end of the DNA. Analytical ultracentrifugation experiments indicate that no more than one molecule of Srs2 is bound to each DNA under these experimental conditions (25 nM $Srs2^{C\Delta276}$ and 50 nM DNA; Figure S2), suggesting that a monomer of Srs2 is sufficient for translocation

Molecular Cell, Vol. 35, No. 1 (July 10, 2009): pg. 105-115. DOI.

on ssDNA. This behavior is similar to that observed for the *E. coli* UvrD translocase (Fischer et al., 2004; Tomko et al., 2007). The rate of Srs2 translocation on ssDNA (approx. 300 nt s^{-1}; Figures 1C & 1D) is significantly faster than the apparent rate of Rad51clearance by Srs2 (approx. 12 nt s^{-1}; Figure 3). The C-terminally deleted proteins $Srs2^{C\Delta 314}$ and $Srs2^{C\Delta 276}$ show similar translocation activities on ssDNA (Figures 1C & 1D; Table S1) yet, as shown below, the $Srs2^{C\Delta 314}$ mutant is selectively defective in clearing Rad51 nucleoprotein filaments.

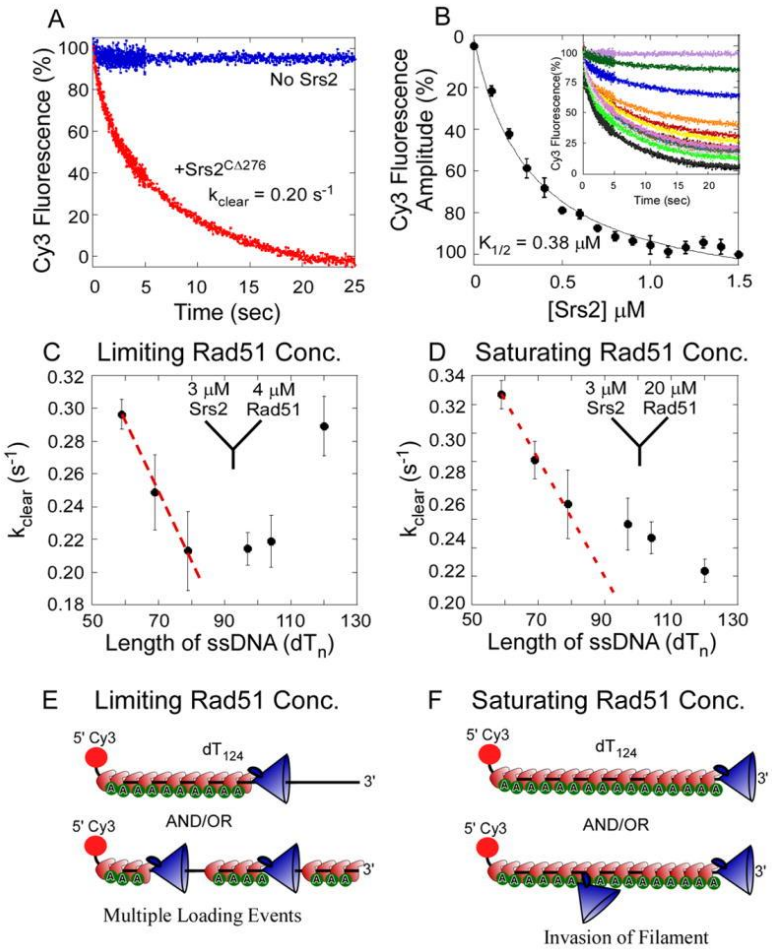

Figure 3: Srs2 Clearing of Rad51 Filaments
(A) In stop flow experiments, preformed Rad51 filaments were rapidly mixed with $Srs2^{C\Delta 276}$. In the absence of Srs2, Rad51 filaments are stable (blue trace), but when challenged with Srs2 (1.5 μM post-mixing) Rad51 filaments are cleared (red trace). (B) $Srs2^{C\Delta 276}$ concentration dependence of Rad51 clearing was measured with increasing concentrations of $Srs2^{C\Delta 276}$ (0 - 1.5 μM post-mixing, shown as insert). The relative change in fluorescence amplitude is plotted as a function of Srs2 concentration and yields a $K_{1/2}$ = 0.38 ± 0.04 μM for Rad51 filament clearing by $Srs2^{C\Delta 276}$. (C) The Rad51 filament clearing experiment in A was repeated with 5'Cy3 ssDNA of varying lengths (dT_n, n = 59-124 nt). Rad51 (2 μM post-mixing) was used in all the

Molecular Cell, Vol. 35, No. 1 (July 10, 2009): pg. 105-115. DOI.

experiments to maintain sub-saturating Rad51-DNA filament forming conditions. The clearing rate observed for each DNA length in the presence of Srs2 (1.5 μM post-mixing) is plotted as a function of DNA length. The red dotted line is the expected trend for the clearing rate if a continuous Rad51-DNA filament is formed under these sub-saturating Rad51 concentrations. (D) The Rad51-DNA filament clearing experiment described in C was repeated with saturating concentrations of Rad51 (10 μM post-mixing). The clearing rates observed under these conditions are plotted as a function of DNA length. The red dotted line represents the expected trend for the clearing rate if Srs2 initiates clearing only at the 3′ end of the Rad51-DNA filament. Deviation from the predicted trend suggests that Srs2 can invade a Rad51 filament at multiple points and initiate clearing. (E) and (F) depict schematic representations of expected Rad51-DNA filaments formed under limiting or saturating concentrations of Rad51, and potential Srs2 loading or invading sites on the respective filaments.

Rad51 Filament Dynamics Are Coupled to ATP Turnover within the Rad51 Filament

We developed a fluorescence-based assay to monitor the kinetics of spontaneous assembly of Rad51 filaments on ssDNA and their disassembly by Srs2. Rad51 was mixed rapidly with ATP and a ssDNA (dT_{79} in length), labeled with Cy3 at the 3′ end or 5′ end, and the resulting increase in Cy3 fluorescence was monitored over time. The change in fluorescence upon Rad51 binding appears to be saturated faster when Cy3 is at the 5′ end compared to the 3′ end of the ssDNA (Figures 2A & 2B). Furthermore, lower concentrations of Rad51 are required to reach maximal fluorescence change with DNA labeled at the 5′ end compared to the 3′ end (Figures 2C & S3A). Differences in the responses to Rad51 monitored at the 5′ or 3′ end of the DNA are suggestive of a directional bias in filament assembly. However, the time courses of filament nucleation and growth display several phases that are indicative of additional complexities that we have not analyzed further.

Molecular Cell, Vol. 35, No. 1 (July 10, 2009): pg. 105-115. DOI.

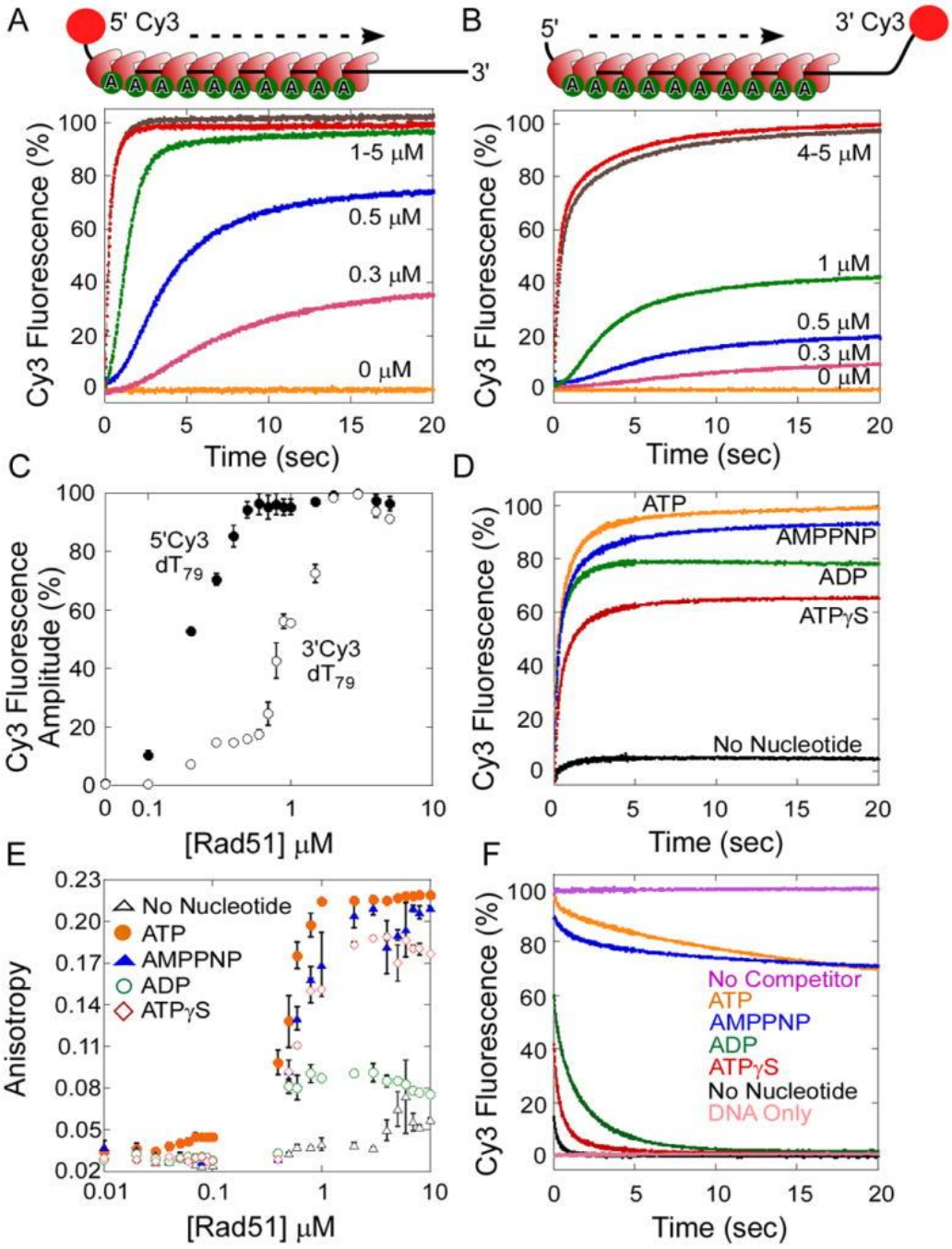

Figure 2: Assembly and Disassembly of Rad51 Filaments on Single Stranded DNA

(A) Kinetics of Rad51 binding to a 5'Cy3 labeled dT_{79} oligonucleotide. Increasing concentrations of Rad51 (0-10 μM) were rapidly mixed with 5'Cy3-dT_{79} ssDNA (40 nM) and ATP-Mg^{2+} (5 mM) using a stopped flow instrument. The change in Cy3 fluorescence measured as a function of time reveals an increase in the Cy3 fluorescence upon Rad51 binding to the DNA. (B) Kinetics of Rad51 binding to a 3'Cy3 labeled dT_{79} oligonucleotide. (C) The change in fluorescence amplitude observed in A

Molecular Cell, Vol. 35, No. 1 (July 10, 2009): pg. 105-115. DOI.

and B are plotted versus the concentration of Rad51 (log scale). Rad51 binds preferentially to the 5′ end (●) compared to the 3′ end (○) of the ssDNA. (D) Rad51 binding to ssDNA requires nucleotide. Rad51 (4 μM) was rapidly mixed with 5′Cy3-dT_{79} (40 nM) in the absence (black) or presence of ATP (yellow), ADP (green), AMP-PNP (blue), or ATPγS (red) (5 mM). Change in Cy3 fluorescence was measured over 25 sec post-mixing. (E) The stoichiometry of Rad51 molecules bound to a 5′-FITC labeled dT_{79} oligonucleotide was measured using fluorescence anisotropy. Increasing concentrations of Rad51 (0–10 μM) were mixed with 5′-FITC labeled dT_{79} oligonucleotide (40 nM), in the absence (△), or presence of ATP (●), ADP (○), AMP-PNP (▲), or ATPγS (◇) (2.5 mM), and the change in fluorescence anisotropy was measured. (F) Disassociation kinetics of nucleotide-bound Rad51 filaments. Preformed Rad51 filaments −Rad51 (4 μM), 5′Cy3-dT_{79} (40 nM), and ATP/ADP/AMP-PNP/ATPγS (5 mM), were rapidly mixed with excess unlabeled dT_{79} (40 μM). Rad51 filaments formed in the presence of ATP (yellow) or AMP-PNP (blue) have longer half-lives: 24.8 s and 55.0 s respectively, compared to ADP (green) or ATPγS bound molecules (red): 0.17 s or 0.09 s respectively. The filaments are stable when not challenged with competitor DNA (black).

Growth of the yeast Rad51 DNA filament is strictly dependent upon nucleotide binding to Rad51, but not on ATP hydrolysis (Bianco et al., 1998). The enhancement of Cy3 fluorescence is observed only when Rad51 and ssDNA are mixed together in the presence of ATP or its analogs AMP-PNP, ATPγS, or ADP (Figure 2D). At saturating nucleotide concentrations, the amplitude of the Cy3 fluorescence intensity change depends upon the identity of the nucleotide, with the largest changes observed in the presence of ATP. Under conditions of stoichiometric Rad51 binding (Figures 2E & S3B), one Rad51 molecule binds to 3-5 nt of ssDNA, consistent with previous reports (Zaitseva et al., 1999). In the presence of saturating ADP, the binding curve does not reach the same maximum level as seen for other nucleotides (Figure 2E), which may reflect a faster dissociation of ADP-bound Rad51 from DNA. Although ATPγS-Rad51 dissociates rapidly from the DNA (Figure 2F), it is reasonably proficient at supporting nucleoprotein filament formation, in comparison to ADP-Rad51 (Figure 2E). This difference may reflect a more favorable association rate and/or cooperative binding by ATPγS-Rad51 to DNA.

The dissociation of Rad51 nucleoprotein filaments was monitored by pre-assembling Rad51-cofactor complexes with 5′-Cy3-dT_{79}DNA then incubating with an excess of unlabeled dT_{79} DNA (Figure 2F). Substantially different half-lives are observed for Rad51-DNA complexes formed with ATP ($t_{1/2}$ = 24.8 ± 0.2 s), AMP-PNP ($t_{1/2}$ = 55.3 ± 0.5 s), ATPγS ($t_{1/2}$ = 0.1 ± 0.1 s) and ADP ($t_{1/2}$ = 0.17 ± 0.1 s) using a 5′ Cy3 labeled DNA substrate. For DNA with a 3′-Cy3 label, the stabilities of Rad51-DNA complexes formed with different cofactors are

ATP ($t_{1/2}$ = 18.8 ± 0.3 s), AMP-PNP ($t_{1/2}$ = 25.1 ± 0.3 s), ATPγS ($t_{1/2}$ = 0.1 ± 0.12 s), and ADP ($t_{1/2}$ = 0.17 ± 0.2 s) (data not shown). These data agree with the previous finding that ATP hydrolysis promotes Rad51 filament disassembly (Bianco et al., 1998; Chi et al., 2006). The observation that the position of the Cy3 fluorophore (5′ or 3′ end) affects the Rad51 dissociation rate suggests either that filament disassembly is faster near the 3′ end of the DNA or that the two Cy3 reporter groups respond differently to proximal Rad51 binding events.

Rad51 Filament Clearing by Srs2

To study the anti-recombinase activity of Srs2, we monitored the kinetics of ATP-bound Rad51 clearance from the 5′-Cy3-dT_{79} DNA (Figure 3A). Rad51-ATP filaments were assembled on the 5′-Cy3-dT_{79} DNA (40 nM) using excess Rad51 (4 μM) and ATP (5 mM). Filaments were mixed with $Srs2^{C\Delta276}$ (3 μM) to initiate clearing, and the resulting decrease in Cy3 fluorescence yielded the apparent rate of filament clearance, k_{clear} = 0.204 ± 0.004 s^{-1} (Figure 3A; see Experimental Procedures). Although the decrease in 5′-Cy3 fluorescence reflects Rad51 displacement from the ssDNA, the change in Cy3 fluorescence likely occurs only after arrival of the translocating Srs2 at the 5′ end of the DNA. Under saturating Srs2 concentrations, the final fluorescence attained after the filament clearing reaction (at long times) is equivalent to the signal for Srs2 alone, indicating that there is no significant rebinding of Rad51 to the ssDNA (Figure S5).

Substoichiometric amounts of Srs2 effectively clear Rad51 filaments (Krejci et al., 2003), and we next examined filament clearing activity with increasing concentrations of Srs2 (Figure 3B). When sub-saturating concentrations of Srs2 are used, higher final Cy3 fluorescence intensity plateaus are observed that suggest inefficient Rad51 clearance and/or rebinding of Rad51 to the cleared DNA. The amplitude of the Cy3 fluorescence change, plotted as a function of Srs2 concentration, yields a $K_{1/2}$ = 0.38 ± 0.002 μM $Srs2^{C\Delta276}$ for the filament clearing activity (Figure 3B). To test whether filament clearing is a catalytic activity of Srs2, and not the result of stoichiometric binding to DNA, we repeated the experiment using a longer dT_{124} substrate (Figure S4). The observed $K_{1/2}$ = 0.40 ± 0.026 μM for dT_{124} is in good agreement with the $K_{1/2}$ value for the shorter dT_{79} filaments.

Molecular Cell, Vol. 35, No. 1 (July 10, 2009): pg. 105-115. DOI.

If a stoichiometric binding model were applicable, we would predict that more Srs2 would be required to block binding of Rad51 on the longer dT_{124} filaments. Instead, our findings are consistent with a catalytic mechanism of Rad51 filament disassembly by Srs2.

In considering how Srs2 initiates Rad51 filament clearance, we considered two possible scenarios in which Srs2 either initiates clearance at the 3' end of the filament or inserts at random internal sites (Figures 3E & F). The initial rates of filament clearing were assayed on DNA of different lengths (dT_n with n = 59 -124 nt) in the presence of a limiting concentration of Rad51 (2 μM post-mixing; Figure 3C) or with saturating amounts of Rad51 (10 μM, post-mixing; Figure 3D). With limiting amounts of Rad51, the longer DNA substrates (dT 87 -124) are not saturated (Figure S3B) and it is likely that multiple clusters of Rad51 polymers exist on the DNA, punctuated by gaps of exposed ssDNA (Modesti et al., 2007). A biphasic dependence of k_{clear} on dT_n is observed (Figure 3C), in which longer DNAs show faster clearance by $Srs2^{C\Delta 276}$ when Rad51 is limiting. This is consistent with Srs2 initiating clearance of Rad51 at multiple internal sites on incompletely formed filaments (Figure 3E), such that k_{clear} first decreases from n= 60 to 80, but then increases for n = 97 to 124 (Figure 3C). In this case, the longer DNAs (n = 97 to 124) show a faster clearance by $Srs2^{C\Delta 276}$ presumably because Rad51 is sub-saturating. With saturating amounts of Rad51, a continual decrease in k_{clear} is observed as a function of increasing DNA length (Figure 3D). However, since under saturating Rad51 conditions (Figure 3D) the observed rates of clearance deviate from a simple linear relationship, this may indicate imperfections in the Rad51 filaments or some limited ability of Srs2 to invade at internal sites within a Rad51 filament (Figure 3F).

A Nonconserved Region of Srs2 is Required for Rad51 Clearing Activity

The C-terminal region of Srs2 physically interacts with Rad51 (Krejci et al., 2003; Papouli et al., 2005) and with sumoylated PCNA (Pfander et al., 2005) at sites of active DNA repair. Residues 1-845 of Srs2 encompass the conserved SF-1 helicase motifs (Figure 1A), whereas the C-terminal residues 846 -1174 are not homologous with

Molecular Cell, Vol. 35, No. 1 (July 10, 2009): pg. 105-115. DOI.

other SF-1 helicases. The $Srs2^{C\Delta276}$ protein spanning residues 1-898 efficiently dismantles Rad51 filaments (Figure 4A), whereas a deletion of an additional 38 C-terminal residues in the $Srs2^{C\Delta314}$ protein (spanning residues 1-860; Figure 1A) almost completely eliminates this Rad51-specific activity (Figure 4B). The shorter $Srs2^{C\Delta314}$ protein is identical to $Srs2^{C\Delta276}$ in all other activities examined, including DNA unwinding, DNA-dependent ATP hydrolysis, DNA binding (data not shown), and ssDNA translocation activities (Figures 1C & D). Hence, the removal of residues 861-898 from Srs2 uncouples its Rad51-dependent filament clearing activity from other DNA-dependent activities. The physical interaction of Srs2 with Rad51 may promote the loading of Srs2 on Rad51 filaments, facilitating recycling of Srs2 onto the DNA under multiple turnover conditions. These findings suggest that the C-terminal region of Srs2 has a unique and specific role in Rad51 clearing and anti-recombinogenic functions.

Molecular Cell, Vol. 35, No. 1 (July 10, 2009): pg. 105-115. DOI.

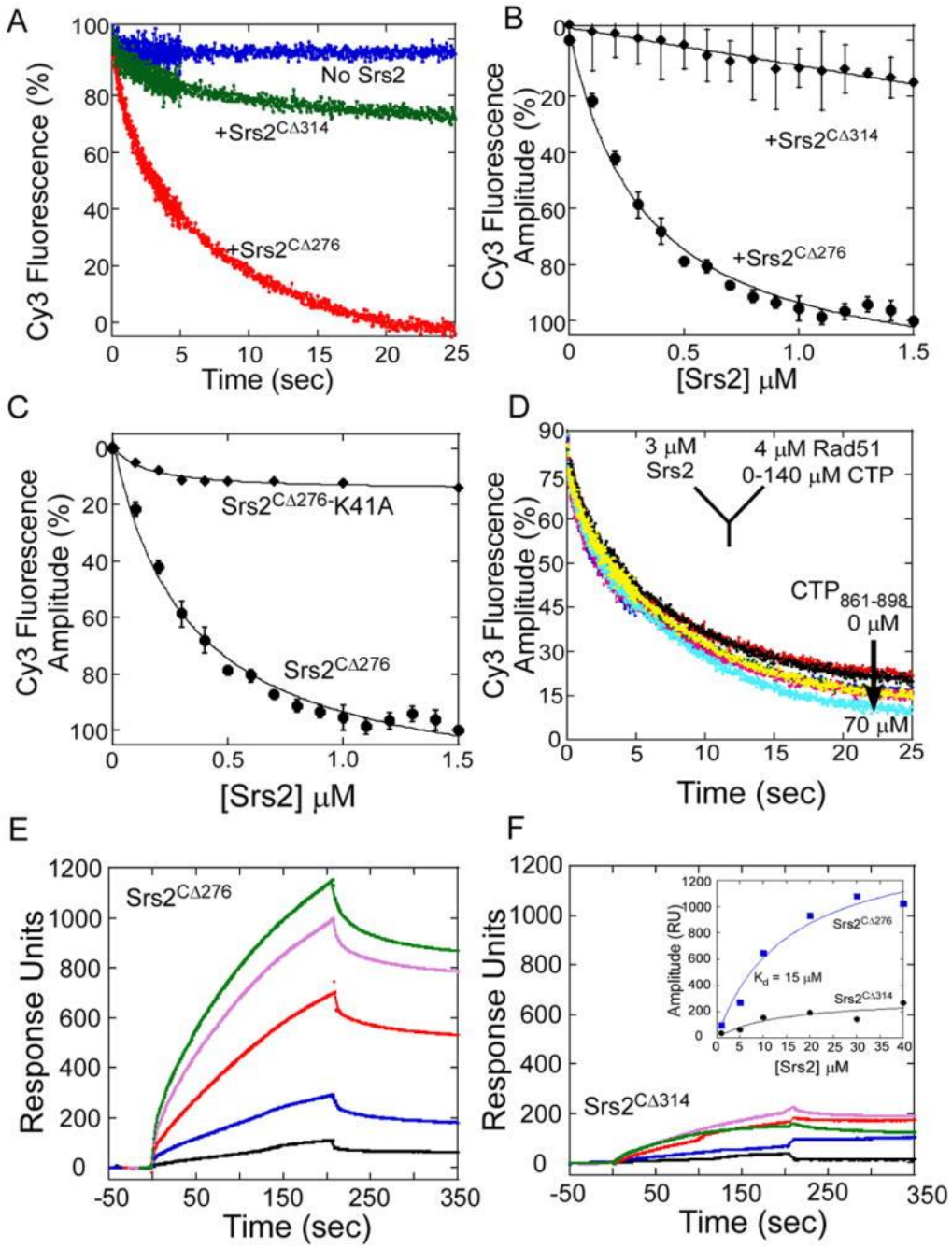

Figure 4: The C-terminus of Srs2 is Essential for its Physical Interaction with Rad51 and Filament Clearing Activity

(A) Pre-formed Rad51-DNA-ATP filaments were rapidly mixed with buffer (blue trace), Srs2$^{C\Delta276}$ (red trace), or Srs2$^{C\Delta314}$ (green trace), and filament clearing monitored as a function of time. Srs2$^{C\Delta314}$, lacking an additional 38 residues is unable to clear a Rad51-DNA filament. (B) Srs2 concentration dependence of filament clearing shows a weak filament clearing activity for Srs2$^{C\Delta314}$ (◆) compared to Srs2$^{C\Delta276}$ (●). (C) An ATP binding/hydrolysis deficient mutant of Srs2$^{C\Delta276}$, Srs2$^{C\Delta276}$-K41A (◆), is unable to clear a preformed Rad51-DNA filament unlike the wild-type Srs2$^{C\Delta276}$ protein (●). (D) A

Molecular Cell, Vol. 35, No. 1 (July 10, 2009): pg. 105-115. DOI.

synthetic peptide corresponding to the Srs2 C-terminal residues 861 – 898, is a poor competitor for $Srs2^{C\Delta276}$ in Rad51 filament clearing experiments. Rad51 was tethered onto a SPR chip, and increasing concentrations of (E) $Srs2^{C\Delta276}$, or (F) $Srs2^{C\Delta314}$ was passed over the chip. The insert shows the change in amplitude (response units, RU) plotted versus the concentration of Srs2, yielding a K_D = 15.2 ± 5 μM for the interaction between $Srs2^{C\Delta276}$ and Rad51. The interaction between $Srs2^{C\Delta314}$ and Rad51 is very weak.

A Physical Interaction between Srs2 and Rad51 is Required for Rad51 Filament Clearing

The physical interaction of Srs2 with Rad51 was monitored on a SPR sensor chip containing immobilized Rad51. The $Srs2^{C\Delta276}$ protein binds to Rad51 with an apparent K_D = 15 ± 5 μM, whereas the $Srs2^{C\Delta314}$ lacking 38 residues at its C-terminus interacts weakly with Rad51 (Figures 4E, & 4F). A synthetic peptide ($CTP_{861\text{-}898}$) corresponding to the region deleted from $Srs2^{C\Delta314}$ did not show an interaction with Rad51 (data not shown) and high concentrations of the peptide failed to inhibit the Rad51 filament clearing activity of $Srs2^{C\Delta276}$ (Figure 4D). These results indicate that the peptide is missing part of the Rad51 protein binding surface or that it fails to fold properly in this context. In addition to the interaction of Srs2 with Rad51, ATP turnover by Srs2 is required for filament clearing. The ATPase defective mutant $Srs2^{C\Delta276}$-K41A binds to ssDNA but fails to clear Rad51 filaments (Krejci et al., 2004)(Figure 4C).

Srs2 Stimulates ATP Hydrolysis within the Rad51 Filament to Promote Clearing

Rad51 nucleoprotein filaments are stabilized by ATP binding (Bianco et al., 1998; Cox et al., 2005; Cox, 2007; Sung and Stratton, 1996) and ATP turnover occurs slowly within the filament (k_{cat} = 0.004 s^{-1}, Table S2), promoting the release of Rad51 from DNA (Figure 2F). We considered the possibility that Srs2 might stimulate ATP turnover by Rad51 in order to achieve the 30- to 50-fold stimulation of Rad51 filament disassembly by Srs2 (k_{clear} ~ 0.2 s^{-1}; Figure 3A). It is difficult to directly measure ATP hydrolysis by Rad51 in the presence of Srs2 because Srs2 hydrolyzes ATP rapidly (80 s^{-1}; data not shown) in the presence of ssDNA.

Molecular Cell, Vol. 35, No. 1 (July 10, 2009): pg. 105-115. DOI.

To determine if ATP turnover by Rad51 limits the filament clearing activity of Srs2, we examined two mutant forms of Rad51. Rad51-K191R hydrolyzes ATP poorly (k_{cat} = 0.001 s^{-1}; Table S2) but is active as a recombinase *in vitro* (Chi et al., 2006; Sung and Stratton, 1996) and *in vivo* (Morgan et al., 2002). Rad51-E221D has a basal rate of ATP hydrolysis (k_{cat} = 0.038 s^{-1}; Table S2) that is 10-fold faster than that of wild-type Rad51. Both mutant Rad51 proteins readily form Rad51 filaments on DNA (Figure 5A) although Rad51-K191R has a 4-fold higher K_D for filament formation (K_D = 0.28 ± 0.005 μM, 0.24 ± 0.004 μM, and 1.21 ± 0.3 μM, for wild-type, E221D, and K191R Rad51 proteins, respectively). The Rad51-K191R protein has been reported to have normal ATP binding activity while being deficient in ATP hydrolysis (Chi et al., 2006; Sung and Stratton, 1996). However, care should be taken when interpreting results obtained with this mutant; since in comparison to wild-type Rad51, the Rad51-K191R protein shows a 90-fold higher $K_{1/2}$ for the ATP dependence of DNA binding (Figure 5B; $K_{1/2}$ = 1.55 ± 0.3 nM, 2.17 ± 0.6 nM, and 140 ± 10 nM for wild-type, E221D, and K191R Rad51 proteins, respectively). Thus, Rad51-K191R appears to show a defect in ATP binding, and requires higher ATP concentrations to form the Rad51-ATP-DNA filaments with this mutant. Nonetheless, with saturating amounts of ATP, the Rad51-K191R and Rad51-E221D proteins efficiently assemble into filaments on ssDNA (Figures 5A & B).

Molecular Cell, Vol. 35, No. 1 (July 10, 2009): pg. 105-115. DOI.

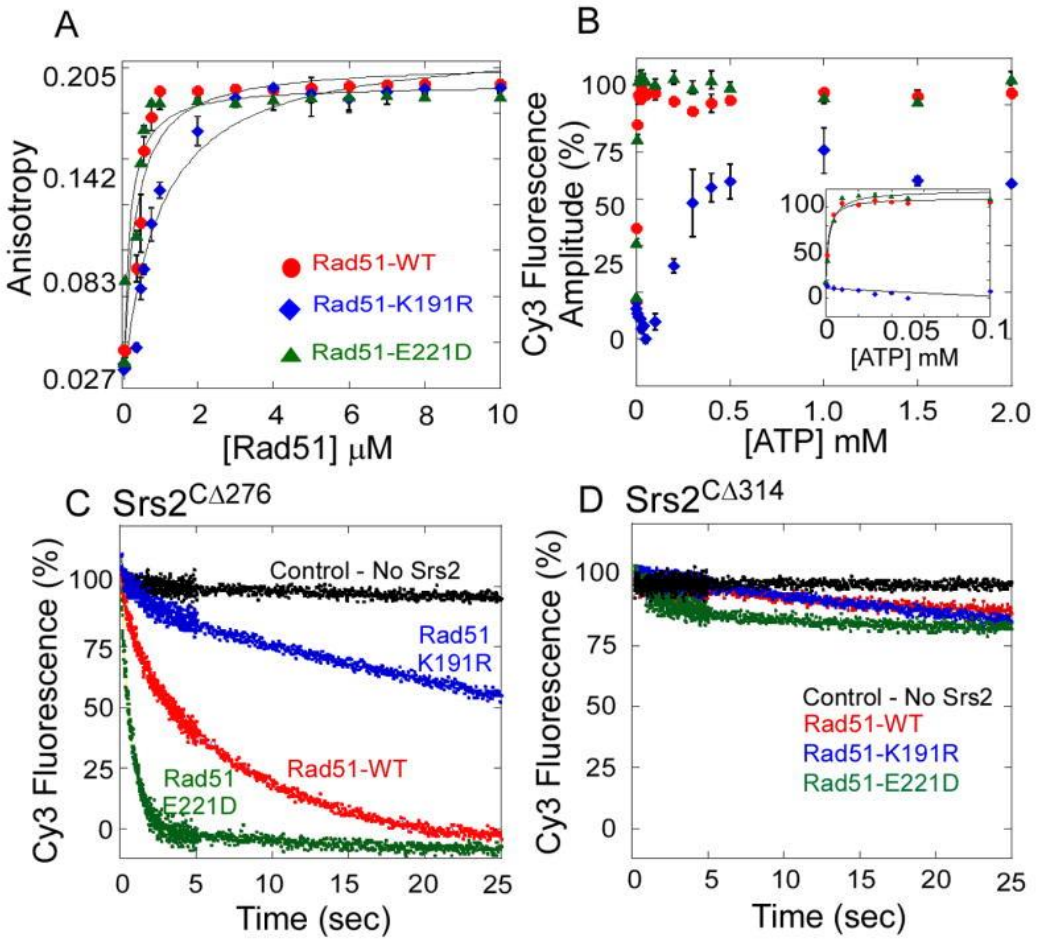

Figure 5: Rad51 Filament Disassembly is Regulated by ATP Hydrolysis Within the Rad51-DNA Filament

(A) Rad51-WT (●), Rad51-K191R (◆), and Rad51-E221D (▲) proteins form a filament on ssDNA measured by fluorescence anisotropy. The ATP hydrolysis deficient mutant (Rad51-K191R) binds ssDNA with lower affinity (K_D = 1.21 ± 0.3 μM) compared to the wild-type Rad51 (K_D = 0.28 ± 0.1 μM) or the Rad51-E221D mutant (K_D = 0.21 ± 0.1 μM). (B) ATP concentration dependence of Rad51 filament formation on ssDNA measured using the stopped flow assay and monitoring changes in 5'Cy3 fluorescence on a dT_{79} DNA substrate. Change in fluorescence amplitude observed at each ATP concentration is plotted for wild-type Rad51 (●), Rad51-K191R (◆), and Rad51-E221D (▲). The $K_{1/2}$ for ATP dependence of filament formation for wild-type Rad51 and Rad51-K191R are 1.5 ± 0.3 nM and 2.1 ± 0.6 nM respectively. The Rad51-K191R mutant (◆) does not bind to DNA at lower ATP concentrations (insert), but forms a filament at higher ATP concentrations ($K_{1/2}$ = 120 ± 28 nM). (C) $Srs2^{C\Delta276}$ clears wild-type Rad51 (red), Rad51-K191R (blue), and Rad51-E221D (green) filaments, but (D) $Srs2^{C\Delta314}$ is incapable of clearing either wild-type Rad51 or mutant Rad51 filaments.

Different rates of Rad51 filament clearing by $Srs2^{C\Delta276}$ are observed for filaments formed by wild-type Rad51 (k_{clear} = 0.204 ± 0.004 s^{-1}), Rad51-E221D (k_{clear} = 1.09 ± 0.04 s^{-1}), and Rad51- K191R (k_{clear} = 0.07 ± 0.01 s^{-1}; Figure 5C). The 5- to 10-fold higher clearance

Molecular Cell, Vol. 35, No. 1 (July 10, 2009): pg. 105-115. DOI.

rate for Rad51-E221D filaments correlates with a 10-fold higher rate of basal ATP hydrolysis by this mutant (Table S2). The clearance of Rad51-K191R filaments occurs at a significantly slower rate (Figure 5C), consistent with the slower basal rate of ATP hydrolysis by Rad51-K191R. This suggests that the rate of enzymatic clearance of Rad51 from DNA appears to be limited by ATP turnover within the Rad51 protein. However, all of these filaments require the enzymatic and Rad51-binding activities of Srs2 to disassemble the filament. The truncated $Srs2^{C\Delta 314}$ protein, which does not interact with Rad51 (Figure 4F), is unable to clear even the destabilized filaments formed by the Rad51-E221D mutant (Figure 5D).

We next examined if Srs2 can modulate ATP turnover by Rad51 to promote filament disassembly. We took advantage of the relatively slow basal rate of ATP turnover in Rad51 bound to ssDNA by assembling filaments in the presence of α-^{32}P-ATP before mixing with $Srs2^{C\Delta 276}$ and a 500-fold molar excess of unlabeled ATP to lower the specific activity of radiolabeled ATP available to bind Srs2. Under these conditions, very little ^{32}P-ADP is formed during a 30 s reaction with $Srs2^{C\Delta 276}$ in the absence of Rad51 (Figure 6A). When Rad51 is preincubated with radiolabeled ATP and dT_{79} ssDNA, the addition of $Srs2^{C\Delta 276}$ causes a concentration-dependent increase in ^{32}P-ATP hydrolysis by Rad51 during filament clearing. Control experiments done with only Rad51, Rad51 + DNA, or Rad51 + $Srs2^{C\Delta 276}$ (in the absence of DNA) showed no detectable ATP hydrolysis during the 30 s incubation (data not shown). A plot of the amount of ^{32}P-ADP formed as a function of $Srs2^{C\Delta 276}$ concentration yields a $K_{1/2}$ = 0.52 ± 0.13 μM Srs2 (Figure 6A), which is comparable to the $K_{1/2}$ = 0.38 ± 0.002 μM for the filament clearing reaction (Figure 3B). Similar experiments done with the mutant Rad51 nucleoprotein filaments (Figure 6C) yield $K_{1/2}$ = 0.90 ± 0.08 (Rad51-K191R) and 0.34 ± 0.02 (Rad51-E221D), indicating that the Rad51-K191R mutant is more resistant to filament clearing by Srs2, whereas the Rad51-E221D mutant is cleared more rapidly than wild-type Rad51. These results suggest that ATP hydrolysis by Rad51 influences the rate of filament clearing by Srs2.

Molecular Cell, Vol. 35, No. 1 (July 10, 2009): pg. 105-115. DOI.

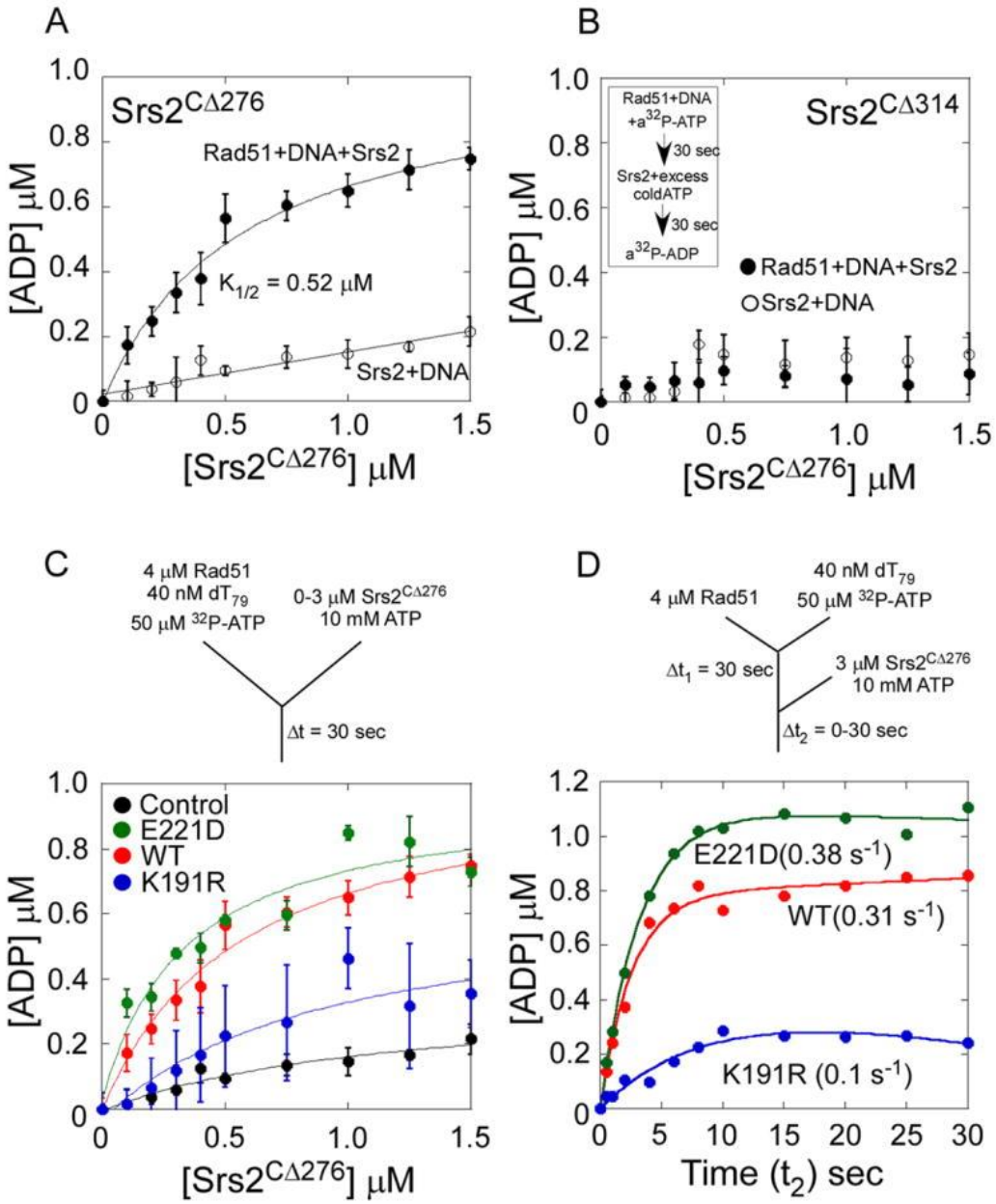

Figure 6: Srs2 Allosterically Stimulates ATP Hydrolysis within the Rad51 Filament Thereby Promoting Filament Disassembly

(A) $Srs2^{C\Delta276}$ stimulates the ATP hydrolysis within a Rad51-DNA filament. Preformed Rad51-DNA-^{32}P-ATP filaments were mixed with increasing concentrations of $Srs2^{C\Delta276}$ and excess unlabeled ATP and the amount of ^{32}P-ADP formed was measured. A stimulation of ATP hydrolysis is observed within the Rad51 filament (●), and the $Srs2^{C\Delta276}$ dependence of this stimulation yields a $K_{1/2}$ = 0.53 ± 0.13 μM. The control experiment done in the absence of Rad51 (○) shows the background level of ^{32}P-ATP hydrolyzed by Srs2 when a 500-fold excess of unlabeled ATP is present. (B) $Srs2^{C\Delta314}$ does not stimulate ATP hydrolysis within a Rad51-DNA filament. The insert shows a schematic representation of the ATPase assays described in A and B. (C) Rad51 filaments were formed on ssDNA (dT_{79}) with either wild-type Rad51 (red), Rad51-

Molecular Cell, Vol. 35, No. 1 (July 10, 2009): pg. 105-115. DOI.

K191R (blue), or Rad51-E221D (green) proteins in the presence of radiolabeled ATP. $Srs2^{C\Delta276}$ stimulates the rate of ATP hydrolysis when added to these filaments along with excess unlabeled ATP. The $Srs2^{C\Delta276}$ dependence of this stimulation yields a $K_{1/2}$ = 0.57 ± 0.15 μM (WT), $K_{1/2}$ = 0.9 ± 0.1 μM (K191R), and $K_{1/2}$ = 0.34 ± 0.07 μM (E221D) respectively. The control experiment done in the absence of Rad51 (black) shows the background level of ^{32}P-ATP hydrolyzed by Srs2 when a 500-fold excess of unlabeled ATP is present. (D) Rate of ATP hydrolysis within the various Rad51 nucleoprotein filaments during filament clearing by $Srs2^{C\Delta276}$ measured using a sequential mixing quenched flow setup. Rad51 (4 μM, WT-red, K191R-blue or E221D-green) was first mixed with dT_{79} DNA (40 nM) and ^{32}P-ATP (50 μM) for 30 seconds and then rapidly mixed with Srs2 (3 μM) and 20 mM excess ATP for varying times (t_2). The schematic for the sequential mixing experiment is shown, and the Srs2 stimulated rates of ATP hydrolysis in the wild-type and mutant Rad51 filaments are noted.

To further quantify the rate of ATP hydrolysis within the Rad51 filament during filament clearing by Srs2, we performed a sequential mixing quenched flow experiment. Modifying the strategy described above, we mixed Rad51 (4 μM) and ^{32}P-ATP for 30 sec (t_1) followed by sequential mixing with Srs2 (3 μM) and a 200 fold excess of unlabeled ATP for varying times (t_2). During filament clearing by Srs2, the wild-type Rad51, Rad51-E221D and Rad51-K191R proteins hydrolyzed ATP at rates of 0.31, 0.38 and 0.1 s^{-1} respectively (Figure 6D).

The stimulated rates of ATP hydrolysis by these Rad51 proteins during filament clearing by Srs2 are 10-fold to 100-fold faster than the basal rates of ATP hydrolysis in the absence of Srs2 (Table S2). We note that the stimulated rates of ATP hydrolysis in Rad51 filaments (Figure 6D) are not equal to the apparent rates of filament clearance (k_{clear}) (Figure 5C); however, this is not expected due to how the clearing rates are measured. In our filament clearing assay, the fluorescence reporter is located at the 5' end of the ssDNA, thus a fluorescence change is detected only from the displacement of Rad51 molecules in the region proximal to the 5' end, rather than displacement of all Rad51 molecules. In contrast, the measured ATPase activity reflects hydrolysis by all Rad51 molecules bound to DNA. Thus, the rates of ATP turnover and Rad51 filament clearance are not expected to be equivalent. Nevertheless, they show the same trends for the different Rad51 mutants.

Despite these caveats, the dose-response curves for Srs2 stimulation of Rad51 ATPase activity ($K_{1/2}$ = 0.57 μM) and filament clearance ($K_{1/2}$ = 0.38 μM) are indeed similar, suggesting that these activities are related mechanistically. Our results show that Srs2

Molecular Cell, Vol. 35, No. 1 (July 10, 2009): pg. 105-115. DOI.

stimulates the rate of ATP hydrolysis within the Rad51 filament, leading to efficient clearing of Rad51 molecules off DNA, and this activity is dependent on its physical interaction with Srs2. Whether this protein-protein interaction is solely required to engage the Rad51 filament or is an active participant in stimulating Rad51's ATPase activity remains to be tested.

UvrD Nonspecifically Antagonizes Rad51 Filaments

The SF-1 helicase/translocase, *E. coli* UvrD, also can disassemble yeast Rad51 filaments (Veaute et al., 2005), although UvrD lacks the C-terminal region of Srs2 that is required for Rad51 binding interactions (Figure 1A). We therefore examined the UvrD concentration dependence for Rad51 filament clearance using the same kinetic assay (Figure 7A). The linear relationship between UvrD concentration and filament clearing activity is consistent with a non-catalytic mechanism for displacement of Rad51. Correspondingly, we do not detect binding of UvrD to Rad51 (Figure 7B), nor does UvrD stimulate ATP hydrolysis by Rad51 during Rad51 filament disassembly (Figure 7C). In addition, high concentrations of UvrD are required to destabilize Rad51 filaments in EM experiments (Figure 7D). These results suggest that UvrD displaces Rad51 by directly competing with Rad51 for DNA binding sites. In contrast, Srs2 uses a catalytic mechanism involving a physical interaction with Rad51 that stimulates ATP turnover and translocation by Srs2 to displace Rad51 from the DNA.

Molecular Cell, Vol. 35, No. 1 (July 10, 2009): pg. 105-115. DOI.

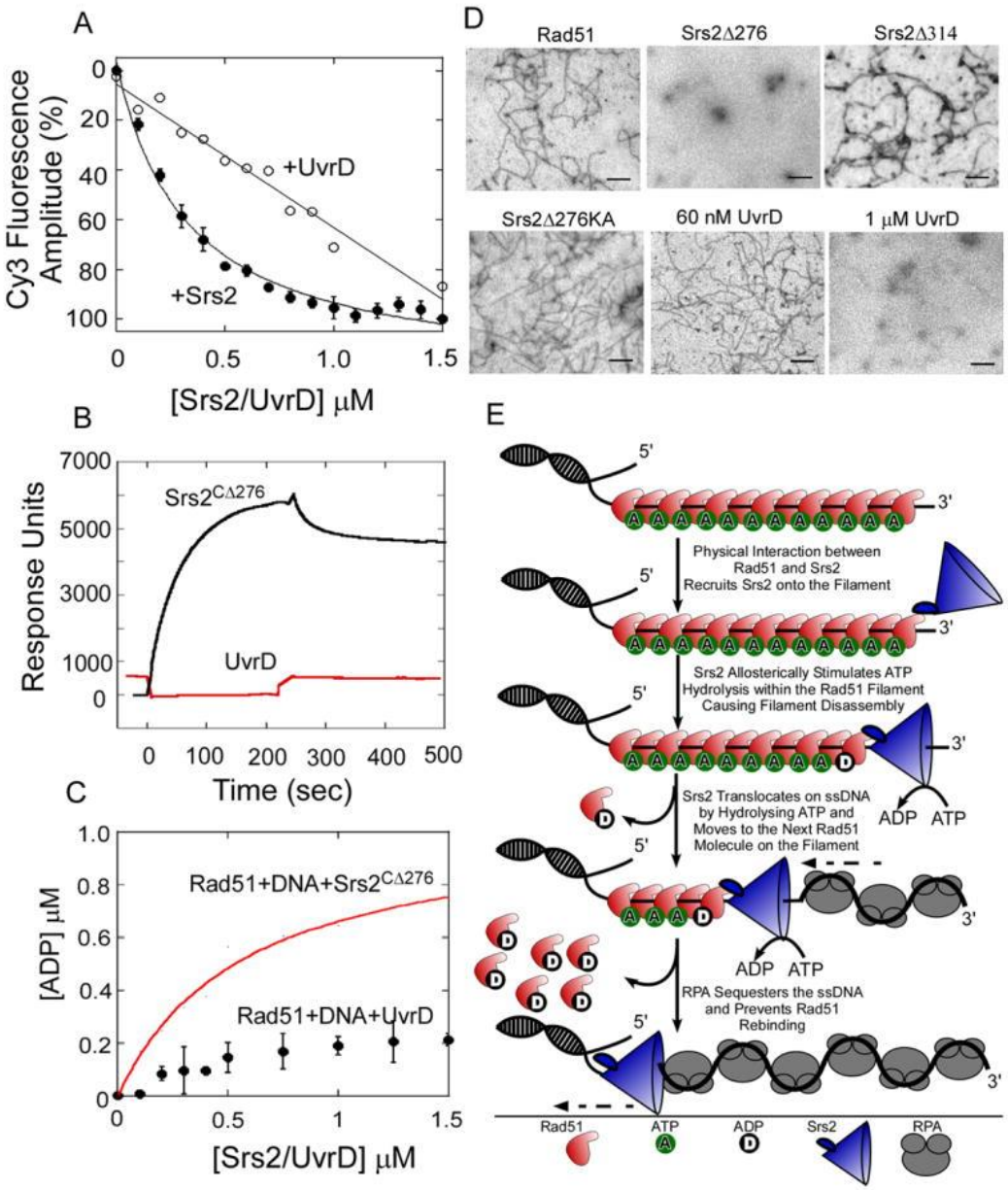

Figure 7: Mechanism of Clearing Rad51 Filaments by Srs2
(A) In stop flow experiments, preformed Rad51 filaments were rapidly mixed with increasing concentrations of Srs2$^{C\Delta276}$ (●) or UvrD (○). The relative change in fluorescence amplitude is plotted as a function of Srs2/UvrD concentration. (B) Rad51 was tethered onto a SPR chip and 7 μM UvrD (red) or Srs2$^{C\Delta276}$ (black) was passed over the chip. The change in response units (RU) is plotted versus time. Srs2$^{C\Delta276}$ binds to Rad51 but no interaction between Rad51 and UvrD is observed. (C) UvrD does not stimulate the rate of ATP hydrolysis within a Rad51-DNA filament (●) unlike Srs2$^{C\Delta276}$ (red trace). (D) EM analysis of Rad51 filaments formed on M13 mp18(+) ssDNA and challenged with RPA, along with 60 nM Srs2$^{C\Delta276}$, Srs2$^{C\Delta314}$, Srs2 Srs2$^{C\Delta276}$ KA, UvrD, or 1 μM UvrD. 60 nM Srs2$^{C\Delta276}$ or 1 μM UvrD are capable of clearing filaments, whereas Rad51 filaments are intact when challenged with 60 nM Srs2$^{C\Delta314}$, Srs2$^{C\Delta276}$ KA, or UvrD. (E) The physical interaction between Srs2 and Rad51 is

Molecular Cell, Vol. 35, No. 1 (July 10, 2009): pg. 105-115. DOI.

required for Srs2 to gain access onto the Rad51 nucleoprotein filament. ATP hydrolysis within the Rad51-DNA filament, allosterically modulated by Srs2, promotes filament disassembly, and the ssDNA translocation activity of Srs2 enables processive 3′ to 5′ clearing of the filament. The free DNA is sequestered by RPA and prevents reformation of the Rad51 filament.

Discussion

Srs2 functions as an anti-recombinase by catalyzing the displacement of the Rad51 recombinase from presynaptic filaments (Krejci et al., 2003; Veaute et al., 2003). It was reasonable to assume that the ATP-dependent motor activity of Srs2 on ssDNA would be sufficient to displace Rad51 from the DNA (Singleton et al., 2007). However, our findings indicate that the Rad51 filament is resistant to clearing by Srs2 when ATP hydrolysis is impaired by mutation of Rad51 (Figure 6C). This suggests that Rad51 is an active participant in the clearing of presynaptic filaments by Srs2. We show that Srs2 stimulates ATP hydrolysis within the Rad51 filament, causing the Rad51 molecules to disassociate from the DNA. A specific protein-protein interaction between the C-terminal region of Srs2 and Rad51 is required for the clearing of presynaptic Rad51 filaments as well as the stimulation of ATP hydrolysis by Srs2. We hypothesize that once Srs2 loads onto the filament through a physical interaction with Rad51, it clears Rad51 filaments by allosterically activating ATP hydrolysis within Rad51 (Figure 7E). In this mechanism of remodeling the Rad51 presynaptic filament, the ATP-dependent ssDNA translocation activity of Srs2 may simply position Srs2 for binding to each successive Rad51 subunit and promote its dissociation from DNA.

Crystal structures of Rad51 and bacterial RecA-type homologs indicate that ATP binds at the interface between subunits of the protein polymer (Conway et al., 2004; Qian et al., 2006; Zhang et al., 2008). The physical interaction of Srs2 with Rad51 may alter packing interactions between Rad51 monomers within the filament, configuring the Rad51 active site for turnover of ATP. The energy required for this conformational change could be contributed by the binding interactions between Srs2 and Rad51, and/or by the mechanical motion of Srs2 on ssDNA. Once a Rad51 molecule is displaced from DNA, Srs2 can translocate along the ssDNA to the next Rad51 subunit in the filament to continue the disassembly process.

Molecular Cell, Vol. 35, No. 1 (July 10, 2009): pg. 105-115. DOI.

Although Srs2 binds to ssDNA with high affinity (K_D = 32 ± 4 nM; data not shown), it is not known how Srs2 loads onto DNA coated with Rad51. The physical interaction of Srs2 with Rad51 might assist loading onto the filament by triggering Rad51 release and providing access to a ssDNA binding site. Once Srs2 is loaded on the DNA, the ssDNA would become available for translocation and processive clearing of Rad51. In addition, the capacity of Srs2 to invade Rad51 filaments at internal sites (Figures 3C, 3D & S4) may increase the efficiency of clearing longer Rad51 filaments several kilobases in length to prevent recombination.

The C-terminal region of Srs2 can be envisioned as a control node that integrates the motor activity of Srs2 with ATP turnover in the Rad51 filament. Srs2 functions in the recovery from checkpoint mediated cell cycle arrest, and several sites of cell cycle-dependent phosphorylation are also located within the C-terminal region of Srs2 (Chiolo et al., 2005). These posttranslational modifications of Srs2 could potentially regulate interactions with Rad51 filaments, enhancing the spatiotemporal control of anti-recombinogenic activity.

Experimental Procedures

Oligonucleotides and Proteins

Unlabeled, Cy3-labeled, and fluorescein isothiocyanate-labeled DNA oligonucleotides were synthesized using an ABI 394 DNA synthesizer and gel purified before annealing. The C-terminal deletion constructs of Srs2, $Srs2^{C\Delta 276}$ and $Srs2^{C\Delta 314}$, were overexpressed in *E. coli* and purified as described (Krejci et al., 2003) with minor modifications (supplemental data). The active site mutant $Srs2^{C\Delta 276}$-K41A was generated using site-directed mutagenesis (Quickchange, Stratagene Inc.), and purified identically. The yRad51 expression plasmid was a kind gift from Dr. Patrick Sung (Yale University) and used to generate mutants of yRad51 by site directed mutagenesis. Both WT and mutant Rad51 proteins were purified as described (Conway et al., 2004). UvrD was purified as described (Runyon et al., 1993) and RPA was a kind gift from Dr. Peter Burgers (Washington University). The Srs2 C-terminal peptide (CTP, residues 861-898) was

Molecular Cell, Vol. 35, No. 1 (July 10, 2009): pg. 105-115. DOI.

synthesized using solid-phase synthesis and purified by HPLC, dried and resuspended in 50 % acetonitrile.

Rad51 Filament Assembly and Dissociation Kinetics

Stopped flow fluorescence experiments were carried out in a SX2000 instrument (Applied Photophysics, UK). The mixing schemes for the various experiments are diagrammed in the respective figures. Equal volumes from both syringes were mixed together at 25 °C, and the change in Cy3 fluorescence was monitored using a 530 nm long pass filter after excitation at 515 nm. All stopped flow experiments were carried out in SF-Buffer (50 mM Tris-Cl, pH 7.5, 10 mM $MgCl_2$, and 50 mM NaCl).

Single strand DNA (Cy3-dT) (oligodeoxythymidylate (dT)) labeled at the 3′ or 5′ terminus with Cy3 (40 nM) and 5 mM ATP were rapidly mixed with increasing concentrations of Rad51 (0 –20 μM). Two control experiments were conducted to normalize the experimental time courses. The ssDNA only control $\left(f_{ssDNA}^{control}(t)\right)$ was obtained by rapidly mixing ssDNA with buffer. The filament control $\left(f_{filament}^{control}(t)\right)$ was obtained by rapidly mixing Rad51:DNA filament with buffer. Each control yielded a constant fluorescence signal that was used to determine the percent change in Cy3 fluorescence for each experimental time course using equation (1).

$$f_{normalized}^{\%}(t) = \left(\frac{f_{obs}\,(t) - f_{ssDNA}^{control}(\infty)}{f_{filament}^{control} - f_{ssDNA}^{control}(\infty)}\right)100 \qquad (1)$$

The effect of nucleotides on Rad51 DNA filament assembly was measured by rapidly mixing a solution of Cy3-dT_{79} (40 nM) and 5 mM nucleotide (ATP, ADP, AMP-PNP, or ATPγS) with Rad51 (4 μM). The fluorescence signal measured in the presence of ATP was considered maximal (100%) relative to the ssDNA only control. The dissociation rate of Rad51 from ssDNA was measured by incubating Rad51 (4 μM), Cy3-dT_{79} (40 nM), and ATP (5 mM) for 1 min then rapidly mixed the solution with excess unlabeled dT_{79} competitor DNA (40 μM). The apparent dissociation rates for the various time courses were

Molecular Cell, Vol. 35, No. 1 (July 10, 2009): pg. 105-115. DOI.

determined by fitting the data to a single exponential (2), where A and k are the amplitude and the rate constant of the fluorescence change corresponding to spontaneous filament disassembly:

$$f^{\%}_{normalized}(t) = A\left(1 - \exp^{(-kt)}\right) \tag{2}$$

Kinetics of Rad51 Filament Clearing by Srs2

Rad51-(Cy3-dT)-ATP filaments were assembled by preincubating Rad51 (4 μM), 5′ or 3′ Cy3-dT_{79} (40 nM), and ATP (5 mM) followed by rapidly mixing with increasing concentrations of Srs2 (0 – 3 μM). Two control experiments were conducted to normalize the experimental time courses as above. In addition to the filament control $\left(f^{control}_{filament}(t)\right)$ a Srs2 disassembled filament control $\left(f^{control}_{Srs\ 2+ssDNA}(t)\right)$ was conducted by preparing a solution of ATP (5 mM), Cy3-dT_{79} (40 nM), and Srs2 (3 μM) then rapidly mixing it with buffer. Each control yielded a constant fluorescence signal (see figure S5) that was used to determine the percent change in Cy3 fluorescence for each filament clearing time course using equation (3).

$$f^{\%}_{normalized}(t) = \left(\frac{f_{obs}(t) - f^{control}_{Srs\ 2+ssDNA}(\infty)}{f^{control}_{filament}(\infty) - f^{control}_{Srs\ 2+ssDNA}(\infty)}\right)100 \tag{3}$$

The filament clearing time courses were analyzed by fitting to a single exponential (1) to obtain an apparent filament clearing rate constant ($k = k_{clear}$) and amplitude change (A). The amplitudes were then plotted as a function of Srs2 concentration and the resulting plot fit to a hyperbola to obtain $K_{1/2}$ values.

We were also able to fit the data reasonably well to a double exponential equation, capturing a rapid but small amplitude component at early time points that is independent of Srs2 concentration and a slower component that consists of the majority of the amplitude change and is dependent on Srs2 concentration. Similar

$K_{1/2}$ values, within error, were obtained with either analysis and the apparent k_{clear} obtained from the single exponential fit was similar to the slower component in the two exponential fits. At this time we do not know what the fast phase is attributed to, but it appears to have little effect on the determined $K_{1/2}$ values and thus the conclusions we have drawn from the data.

The clearing rates for Rad51-K191R and Rad51-E221D were measured similarly by pre-forming Rad51-(Cy3-dT))-ATP filaments with Rad51-K191R or Rad51-E221D (4 μM), Cy3-dT_{79} (40 nM), and ATP (5 mM) and rapidly mixed with Srs2 (3 μM). To study the effects of saturating or limiting concentrations of Rad51 on filament clearance by Srs2, Rad51 filaments were pre-formed with Cy3-dT_{79} (40 nM), ATP (5 mM), and either 4 μM or 20 μM Rad51, then rapidly mixed with Srs2 (3 μM). The apparent filament clearing rates for the various traces were measured by fitting the data to equation (1).

Srs2 ssDNA Translocation Kinetics

Srs2 ssDNA translocation experiments were performed under single round conditions (no rebinding of Srs2 to ssDNA) using a fluorescence stopped-flow assay to monitor the arrival of Srs2 at the 5'-end of the DNA using 5'-Cy3-$(dT)_L$ substrates of various lengths (L) as described (Fischer et al., 2004). For ssDNA translocation assays, $Srs2^{C\Delta 276}$ or $Srs2^{C\Delta 314}$ (25 nM, final) was pre-incubated with excess ssDNA (50 nM, final) in one syringe and reactions initiated by rapid mixing with buffer containing ATP (0.5 mM, final) and heparin (4 mg/ml, final). Heparin functions as a trap to sequester the Srs2 molecules as they dissociate from the DNA ends after a single round of translocation. All concentrations are denoted as the final concentrations, post-mixing. Analysis of the resulting time courses is discussed in supplemental experimental procedures.

SPR Analyses of Rad51-Srs2 Interactions

0.2 mg/ml of Rad51 or BSA (final volume of 100 μl in 10 mM sodium acetate, pH 4.0) was coupled to a sensor chip derivatized with 0.05 M N-hydroxysuccinimide and N-ethyl-N'-(dimethylaminopropyl)carbodiimide, and equilibrated in BC-Buffer (50

Molecular Cell, Vol. 35, No. 1 (July 10, 2009): pg. 105-115. DOI.

mM Tris-Cl, pH 8.0, 0.5 mM EDTA, pH 8.0, 10 % glycerol, 150 mM NaCl, 5 mM β-mercaptoethanol, and 0.01 % NP-40). Increasing concentrations of Srs2 (0 – 40 μM; or 7 μM UvrD) in 100 μl reaction volume were passed over the chip. The increase in response units (RU) was measured over 200 seconds during the binding reaction, followed by washing with BC buffer and monitoring disassociation for an additional 200 seconds. The chip was regenerated in between runs with a mixture of 10 μl 0.2 %SDS and 10 mM NaOH. The change in RU at $\Delta T = 0$ sec was subtracted from RU at $\Delta T = 200$ sec to obtain the change in amplitude. The RU amplitude change was plotted against Srs2 concentration and fit to a hyperbola to obtain a K_D for the interaction.

ATPase Assays

To analyze the $K_{1/2}$ for ATP hydrolysis within the Rad51 filament, 50 μM of α^{32}P-ATP was mixed with 2 μM Rad51 and 40 nM dT_{79} DNA in 10 μl reactions in ATPase buffer (120 mM Tris-Cl, pH7.5, 50 mM NaCl, 10 mM $MgCl_2$, 0.5 mM βME, and 100 μg/ml BSA) and incubated for 30 seconds at 25 °C. Different concentrations of Srs2 (0 – 1.5 μM) was added along with 25 mM unlabeled ATP-Mg^{2+}. The reaction was incubated for an additional 30 seconds, and stopped by adding 10 μl of 0.5 M EDTA. ADP formation was monitored by spotting 1 μl of the reaction on a TLC plate, dried, and resolved with 0.6 M phosphate buffer (pH 3.4).

The rate of ATP hydrolysis during filament clearing was measured on a KinTek Quenched Flow System using a sequential mixing setup. To form the nucleoprotein filaments, equal volumes (18 μl each) of 4 μM Rad51, 40 nM dT_{79} DNA and 50 μM ^{32}P-ATP in the SF-Buffer were rapidly mixed for 30 sec (t_1) during the first mixing. This reaction was then sequentially mixed for varying times ($t_2 = 0 – 30$ sec) with 3 μM $Srs2^{C\Delta 276}$. The reaction was quenched with 70 μl quench solution (1M HCl), neutralized with 27 μl neutralization buffer (2.5 M NaOH, 0.5 M EDTA and 0.5 M Tris). ADP formation was monitored by spotting 1 μl of the reaction on a TLC plate, dried, and resolved with 0.6 M phosphate buffer (pH 3.4).

Molecular Cell, Vol. 35, No. 1 (July 10, 2009): pg. 105-115. DOI.

Electron Microscopy

EM analyses of Rad51 filaments were performed as described (Krejci et al., 2003). Srs2 or UvrD (60 nM or 1 μM) were mixed with RPA (350 nM) then added to Rad51 filaments assembled on M13mp18(+) ssDNA (2.4 μM Rad51; 7.5 μM nucleotides in M13 DNA) in EM buffer (50 mM Tris-Cl, pH 7.5, 150 mM NaCl, 10 % glycerol and 0.5 mM EDTA) and incubated at 37 °C for 3 minutes. 3 μl of the reaction was spotted onto freshly glow discharged carbon-coated copper grids for 2 min. The grids were rinsed two times in R buffer and stained with 0.75% uranyl formate (Electron Microscopy Sciences, Hatfield, PA) for 30 sec. Excess liquid was wicked away and the grids were allowed to air dry. Samples were viewed on a JEOL 1200EX transmission electron microscope (JEOL USA, Peabody, MA). Images were acquired at 40,000x or 60,000x magnification.

Acknowledgments

We thank Patrick Sung for the kind gift of the yRad51 protein overexpression plasmid, Jurek Majka, and Bill Nolan for assistance with experiments, and Wandy Beatty for the EM analysis. This work was supported by research grants to TE (R01GM059902 and NCI-PO1CA092584), TML (GM045948), and LK (WT076476).

Abbreviations

HR Homologous Recombination
DSBs Double Stranded Breaks
ssDNA Single Stranded DNA
dsDNA Double Stranded DNA
nt nucleotide
bp base pair
aa amino acid

Footnotes

Publisher's Disclaimer: This is a PDF file of an unedited manuscript that has been accepted for publication. As a service to our customers we are providing this early version of the manuscript. The manuscript will undergo copyediting, typesetting, and review of the resulting proof before it is published in its final

citable form. Please note that during the production process errors may be discovered which could affect the content, and all legal disclaimers that apply to the journal pertain.

References

Bianco PR, Tracy RB, Kowalczykowski SC. DNA strand exchange proteins: a biochemical and physical comparison. *Front Biosci*. 1998;3:D570–603.

Bugreev DV, Yu X, Egelman EH, Mazin AV. Novel pro- and anti-recombination activities of the Bloom's syndrome helicase. *Genes Dev*. 2007;21:3085–3094.

Chi P, Van Komen S, Sehorn MG, Sigurdsson S, Sung P. Roles of ATP binding and ATP hydrolysis in human Rad51 recombinase function. *DNA Repair* (Amst) 2006;5:381–391.

Chiolo I, Carotenuto W, Maffioletti G, Petrini JH, Foiani M, Liberi G. Srs2 and Sgs1 DNA helicases associate with Mre11 in different subcomplexes following checkpoint activation and CDK1-mediated Srs2 phosphorylation. *Mol Cell Biol*. 2005;25:5738–5751.

Conway AB, Lynch TW, Zhang Y, Fortin GS, Fung CW, Symington LS, Rice PA. Crystal structure of a Rad51 filament. *Nat Struct Mol Biol.* 2004;11:791–796.

Cox JM, Tsodikov OV, Cox MM. Organized unidirectional waves of ATP hydrolysis within a RecA filament. *PLoS Biol*. 2005;3:e52.

Cox MM. Regulation of bacterial RecA protein function. *Crit Rev Biochem Mol Biol.* 2007;42:41–63.

Fischer CJ, Maluf NK, Lohman TM. Mechanism of ATP-dependent translocation of E.coli UvrD monomers along single-stranded DNA. *J Mol Biol*. 2004;344:1287–1309.

Hu Y, Raynard S, Sehorn MG, Lu X, Bussen W, Zheng L, Stark JM, Barnes EL, Chi P, Janscak P, et al. RECQL5/Recql5 helicase regulates homologous recombination and suppresses tumor formation via disruption of Rad51 presynaptic filaments. *Genes Dev*. 2007;21:3073–3084.

Korolev S, Hsieh J, Gauss GH, Lohman TM, Waksman G. Major domain swiveling revealed by the crystal structures of complexes of E. coli Rep helicase bound to single-stranded DNA and ADP. *Cell*. 1997;90:635–647.

Krejci L, Macris M, Li Y, Van Komen S, Villemain J, Ellenberger T, Klein H, Sung P. Role of ATP hydrolysis in the antirecombinase function of Saccharomyces cerevisiae Srs2 protein. *J Biol Chem*. 2004;279:23193–23199.

Krejci L, Van Komen S, Li Y, Villemain J, Reddy MS, Klein H, Ellenberger T, Sung P. DNA helicase Srs2 disrupts the Rad51 presynaptic filament. *Nature*. 2003;423:305–309.

Krogh BO, Symington LS. Recombination proteins in yeast. *Annu Rev Genet*. 2004;38:233–271.

Lee JY, Yang W. UvrD helicase unwinds DNA one base pair at a time by a two-part power stroke. *Cell*. 2006;127:1349–1360.

Li X, Heyer WD. Homologous recombination in DNA repair and DNA damage tolerance. *Cell Res*. 2008;18:99–113.

Lohman TM, Tomko EJ, Wu CG. Non-hexameric DNA helicases and translocases: mechanisms and regulation. *Nat Rev Mol Cell Biol.* 2008;9:391–401.

Modesti M, Ristic D, van der Heijden T, Dekker C, van Mameren J, Peterman EJ, Wuite GJ, Kanaar R, Wyman C. Fluorescent human RAD51 reveals multiple nucleation sites and filament segments tightly associated along a single DNA molecule. *Structure*. 2007;15:599–609.

Morgan EA, Shah N, Symington LS. The requirement for ATP hydrolysis by Saccharomyces cerevisiae Rad51 is bypassed by mating-type heterozygosity or RAD54 in high copy. *Mol Cell Biol*. 2002;22:6336–6343.

Papouli E, Chen S, Davies AA, Huttner D, Krejci L, Sung P, Ulrich HD. Crosstalk between SUMO and ubiquitin on PCNA is mediated by recruitment of the helicase Srs2p. *Mol Cell*. 2005;19:123–133.

Pellegrini L, Venkitaraman A. Emerging functions of BRCA2 in DNA recombination. *Trends Biochem Sci*. 2004;29:310–316.

Pfander B, Moldovan GL, Sacher M, Hoege C, Jentsch S. SUMO-modified PCNA recruits Srs2 to prevent recombination during S phase. *Nature*. 2005;436:428–433.

Qian X, He Y, Ma X, Fodje MN, Grochulski P, Luo Y. Calcium stiffens archaeal Rad51 recombinase from Methanococcus voltae for homologous recombination. *J Biol Chem*. 2006;281:39380–39387.

Rong L, Klein HL. Purification and characterization of the SRS2 DNA helicase of the yeast Saccharomyces cerevisiae. *J Biol Chem.* 1993;268:1252–1259.

Runyon GT, Wong I, Lohman TM. Overexpression, purification, DNA binding, and dimerization of the *Escherichia coli* uvrD gene product (helicase II) *Biochemistry*. 1993;32:602–612.

Singleton MR, Dillingham MS, Wigley DB. Structure and mechanism of helicases and nucleic acid translocases. *Annu Rev Biochem.* 2007;76:23–50.

Sung P, Klein H. Mechanism of homologous recombination: mediators and helicases take on regulatory functions. *Nat Rev Mol Cell Biol*. 2006;7:739–750.

Sung P, Stratton SA. Yeast Rad51 recombinase mediates polar DNA strand exchange in the absence of ATP hydrolysis. *J Biol Chem.* 1996;271:27983–27986.

Symington LS. Role of RAD52 epistasis group genes in homologous recombination and double-strand break repair. *Microbiol Mol Biol Rev*. 2002;66:630–670. table of contents.

Thorslund T, West SC. BRCA2: a universal recombinase regulator. *Oncogene*. 2007;26:7720–7730.

Tomko EJ, Fischer CJ, Niedziela-Majka A, Lohman TM. A nonuniform stepping mechanism for E. coli UvrD monomer translocation along single-stranded DNA. *Mol Cell*. 2007;26:335–347.

Veaute X, Delmas S, Selva M, Jeusset J, Le Cam E, Matic I, Fabre F, Petit MA. UvrD helicase, unlike Rep helicase, dismantles RecA nucleoprotein filaments in *Escherichia coli*. *EMBO J*. 2005;24:180–189.

Veaute X, Jeusset J, Soustelle C, Kowalczykowski SC, Le Cam E, Fabre F. The Srs2 helicase prevents recombination by disrupting Rad51 nucleoprotein filaments. *Nature*. 2003;423:309–312.

Velankar SS, Soultanas P, Dillingham MS, Subramanya HS, Wigley DB. Crystal structures of complexes of PcrA DNA helicase with a DNA substrate indicate an inchworm mechanism. *Cell*. 1999;97:75–84.

Zaitseva EM, Zaitsev EN, Kowalczykowski SC. The DNA binding properties of Saccharomyces cerevisiae Rad51 protein. *J Biol Chem*. 1999;274:2907–2915.

Zhang D, Chen C, Fu X, Gu S, Mao Y, Xie Y, Huang Y, Li Y. A meta-analysis of DNA repair gene XPC polymorphisms and cancer risk. *J Hum Genet*. 2008;53:18–33.

Supplemental Data

I. Supplemental Experimental Procedures

Purification of Srs2

DNAs encoding the C-terminal deletion constructs, $Srs2^{C\Delta 276}$ and $Srs2^{C\Delta 314}$, were cloned into pET11a with a 9x N-terminal histidine tag using NdeI and BamHI restriction sites. These proteins were overexpressed in *E. coli* BL21 Rossetta-2 cells. Following growth to an OD_{600} 0.6 at 37°C, the cultures were transferred to 16°C and protein expression was induced overnight with 0.4 mM IPTG. Cells from a 10 L culture were resuspended in 250 Buffer-I (100 mM KH_2PO_4, pH 8.0, 1 mM PMSF, 10 mM protease inhibitor cocktail, 10 % glycerol, 500 mM NaCl, 1 M Urea and 10 mM β-mercaptoethanol). All subsequent steps were carried out at 4°C. Cells were lysed using a cell disrupter (Avestin Inc.), and Srs2 was precipitated by adding 0.26 g/ml ammonium sulfate to the clarified supernatant. The ammonium sulfate pellet was slowly resuspended in 250 ml Buffer-II (100 mM KH_2PO_4, pH 8.0, 1 mM PMSF, protease inhibitor cocktail, 10 % glycerol, 500 mM NaCl, 1 M Urea, and 20 mM imidazole), and fractionated over a 15 ml Ni^{2+}-NTA column equilibrated with Buffer-II. After binding Srs2 to the

Molecular Cell, Vol. 35, No. 1 (July 10, 2009): pg. 105-115. DOI.

column, it was washed extensively with 500 ml Buffer-III (100 mM KH_2PO_4, pH 8.0, 1 mM PMSF, protease inhibitor cocktail, 10 % glycerol, 500 mM NaCl and 20 mM imidazole) to remove the urea and non-specifically bound proteins. Srs2 was eluted using a 150 ml linear gradient (20 mM to 700 mM Imidazole in Buffer-III). Fractions containing Srs2 were pooled and diluted to a conductivity corresponding to 400 mM NaCl with Buffer-IV (50 mM Tris-Cl, pH 8.0, 0.5 mM EDTA, protease inhibitor cocktail, 5 mM β mercaptoethanol, 10 % glycerol). The diluted protein was further fractionated on a 10 ml Q-Sepharose column (equilibrated with Buffer-IV+200 mM NaCl). The procedure was designed to reduce the final conductivity to correspond to 200 mM NaCl immediately before the solution was applied to the resin. Under these conditions, Srs2 flows through the Q-Sepharose column. The flow through fraction was diluted to a final conductivity of 150 mM and fractionated further on a 10 ml Hi-Trap Heparin column (equilibrated with Buffer-IV+50 mM NaCl). Srs2 was eluted with a 110 ml linear gradient (200 mM – 800 mM NaCl in Buffer-IV). Fractions containing Srs2 were pooled, concentrated to a final volume of 4 ml, and fractionated on a S200 gel filtration column in Buffer-VI (50 mM Tris-Cl, pH 8.0, 0.5 mM EDTA, 5 mM β mercaptoethanol, 20 % glycerol and 150 mM NaCl). Fractions containing Srs2 were pooled and concentrated to a final concentration of 12 mg/ml and aliquots were flash frozen in liquid nitrogen and stored at -80°C.

Analytical Gel Filtration

To analyze the aggregation state of Srs2 in solution, 10 µl of 0.5 mg/ml or 10 mg/ml $Srs2^{C\Delta276}$ or $Srs2^{C\Delta314}$ in Buffer-VI was chromatographed on a Superose-12 column. 10 µl of 0.5 mg/ml molecular weight standards (blue dextran, aldolase, ovalbumin and ribonucleaseA) were also analyzed in Buffer-VI.

Analytical ultracentrifugation

Analytical sedimentation equilibrium experiments were performed using a ProteomeLab XL-A analytical ultracentrifuge equipped with a 50Ti rotor (Beckman Coulter, Fullerton, CA) at 25°C in SF-Buffer (50 mM Tris-HCl, pH 7.5, 10 mM $MgCl_2$ and 50 mM NaCl). Varying molar ratios of $Srs2^{\Delta C276}$ to ssDNA were prepared in SFBuffer. The ssDNA was dT_{79} nt in length, covalently labeled at the 5′ end with Cy3 (5′-Cy3-dT79). Absorbance data were collected by scanning the sample cells at 550 nm at intervals of 0.001 cm in the step mode with seven averages per step. Samples (120 µl) were loaded into each of the three channels of an Epon charcoal-filled six-channel centerpiece and buffer (122 µl) was used to fill the reference chambers. Two different molar ratios of $Srs2^{\Delta C276}$ to DNA were used in the

Molecular Cell, Vol. 35, No. 1 (July 10, 2009): pg. 105-115. DOI.

experiment that was conducted at three different rotor speeds (15,000; 18,000; and 22,000 rpm), starting with the lowest and finishing with the highest speed. Attainment of equilibrium at each speed was judged by the superimposability of three successive scans taken 2 hours apart. The sedimentation equilibrium data were edited using the program REEDIT (Jeff Lary, National Analytical Ultracentrifugation Center, Storrs, CT) and the resulting absorbance profiles were globally fit to equation (1) using the nonlinear least-squares routine in Conlin (1).

$$A_T = \sum_{i-1}^{\eta} \exp\left(\ln A_{0,i} + \sigma_i \left(r^2 - r_{ref}^2\right) / 2\right) + b \qquad (1)$$

In equation (1) A_T is the total absorbance at radial position, r; $A_{0,i}$ is the absorbance of component i at the reference radial position (r_{ref}); b is baseline offset; σi is the reduced molecular mass of component i, which is equal to $[M_i(1 - \bar{\upsilon}\, i\rho)\omega^2] / RT$; M$i$ is the molecular mass of component i; $\bar{\upsilon}\, i$ is the partial specific volume of component i at experimental temperature; ρ is buffer density at experimental temperature; ω is the angular velocity of the rotor; T is the absolute temperature; R is the gas constant. Buffer density (ρ), Srs2$^{\Delta C276}$ molecular mass, and Srs2$^{\Delta C276}$ partial specific volume was calculated at 25°C using the Sedenterp software (Laue, 1992)(ρ = 1.00239 g/ml, $M_{Srs2\Delta C276}$ = 103247.8 g/mol, and $\bar{\upsilon}_{Srs2\Delta C276}$ = 0.7411 ml/g). The model yielding the best fit (eq. (1), n = 2) assumed the presence of two species in solution: free ssDNA and Srs2:ssDNA complex. The data was fit by constraining the parameters for free ssDNA in solution ($\bar{\upsilon}_{5'\text{-Cy3-dT79}}$) and floating for the molecular mass of the Srs2:ssDNA complex, assuming a weight average $\bar{\upsilon}$ for the Srs2:ssDNA complex (calculated values: $\bar{\upsilon}_{S:D}$=0.7015 ml/g, $\bar{\upsilon}_{S2:D}$=0.7192 ml/g, and $\bar{\upsilon}_{S3:D}$=0.7260).

The partial specific volume of the ssDNA ($\bar{\upsilon}_{5'\text{-Cy3-dT79}}$) in solution was determined experimentally in an independent sedimentation experiment. ssDNA (1.4 μM) was sedimented to equilibrium at four successive rotor speeds (15,000; 18,000; 22,000; and 26,000) in SF-buffer at 25°C. The absorbance profiles were globally fit using WinNonlin (Johnson et al., 1981) assuming a single ideal species model (n=1 in eq. (1)). From the best-fit value of the reduced molecular mass, σi, the partial specific volume was determined assuming a molecular mass of the ssDNA equal to the value calculated from its composition. ($M_{5'Cy3\text{-}dT79}$= 24476.1 g/mol, $\bar{\upsilon}_{5'Cy3\text{-}dT79}$= 0.535±0.012 ml/g). The uncertainties (95% confidence limits) in the fitted parameters were determined by performing a 100-cycle Monte Carlo

Molecular Cell, Vol. 35, No. 1 (July 10, 2009): pg. 105-115. DOI.

(Straume and Johnson, 1992) simulation routine in Conlin (Williams and Hall, 2000).

Analysis of the Srs2 monomer ssDNA translocation time courses

The Srs2 monomer ssDNA translocation time courses in Figures 1C, and 1D were analyzed by NLLS analysis using an n-step sequential model and the software Conlin (Williams and Hall, 2000), as previously described (Fischer et al., 2004). The dissociation rate constant from internal sites, *kd*, was constrained in the analysis to the value determined independently by monitoring dissociation from poly(dT) as described (Fischer et al., 2004) (data not shown, value reported in Table S1). The uncertainties in the fitted parameters represent 68% confidence limits and were determined by performing a 100-cycle Monte Carlo simulation (Straume and Johnson, 1992) routine in Conlin (Williams and Hall, 2000). At this time we are reporting the macroscopic translocation kinetic parameters for each Srs2 truncation (Table S1). These parameters are not affected by the fluorophore used in the experiment and can be readily determined from the global analysis of a series of translocation time courses obtained on different length ssDNA labeled with a fluorophore (Cy3 in this case), using a n-step sequential model. The values of the microscopic kinetic parameters, such as the kinetic step size, can be affected by choice of fluorophore, requiring the global analysis of additional sets of translocation time courses obtained with ssDNA labeled with a different fluorophore (Fischer et al., 2004). We are currently conducting experiments using different fluorophores to obtain fluorophore independent estimates of the microscopic kinetic parameters.

Supplementary References

Fischer, C.J., Maluf, N.K., and Lohman, T.M. (2004). Mechanism of ATP-dependent translocation of *E. coli* UvrD monomers along single-stranded DNA. *J Mol Biol 344*,1287-1309.

Johnson, M.L., Correia, J.J., Yphantis, D.A., and Halvorson, H.R. (1981). Analysis of data from the analytical ultracentrifuge by nonlinear least-squares techniques. *Biophys J 36*, 575-588.

Laue, T.M., Shah, B.D, Ridgeway, T.M. and Pelletier, S.L. (1992). Computer-aided interpretation of analytical sedimentation data for proteins. In *Royal Society of Chemistry*, Cambridge, UK, pp. 90-125

Straume, M., and Johnson, M.L. (1992). Monte Carlo method for determining complete confidence probability distributions of estimated model parameters. *Methods Enzymol 210*, 117-129.

Williams, D.J., and Hall, K.B. (2000). Monte Carlo applications to thermal and chemical denaturation experiments of nucleic acids and proteins. *Methods Enzymol 321*, 330-352.

Table S1.

Table S1: ssDNA translocation kinetic parameters for Srs2 monomer

Translocation kinetic parameter	$Srs2^{C\Delta 276}$	$Srs2^{C\Delta 314}$
Translocation rate (nts s^{-1})	298 ± 3	301 ± 5
k_d (s^{-1})[a]	0.19 ± 0.01	0.19 ± 0.01
Processivity: 1/(1-*P*) (nts) (4 mg/ml heparin)[b]	1570 ± 17	1561 ± 24

[a] Measured independently in assay using Poly(dT). The parameter was constrained in the NLLS analysis of the translocation time courses.
[b] Average number of nucleotides translocated before dissociation in the presence of heparin (protein trap). P = (*Translocation rate)*/(*Translocation rate* + k_d) (ssDNA translocation processivity)

Molecular Cell, Vol. 35, No. 1 (July 10, 2009): pg. 105-115. DOI.

Table S2.

Basal and Srs2-stimulated ATPase Rates of Rad51

	WT	K191R	E221D
Basal ATPase Rate (s^{-1})	0.004	0.001	0.038
Stimulated ATPase Rate (s^{-1})	0.31	0.10	0.38

Molecular Cell, Vol. 35, No. 1 (July 10, 2009): pg. 105-115. DOI.

Figure S1

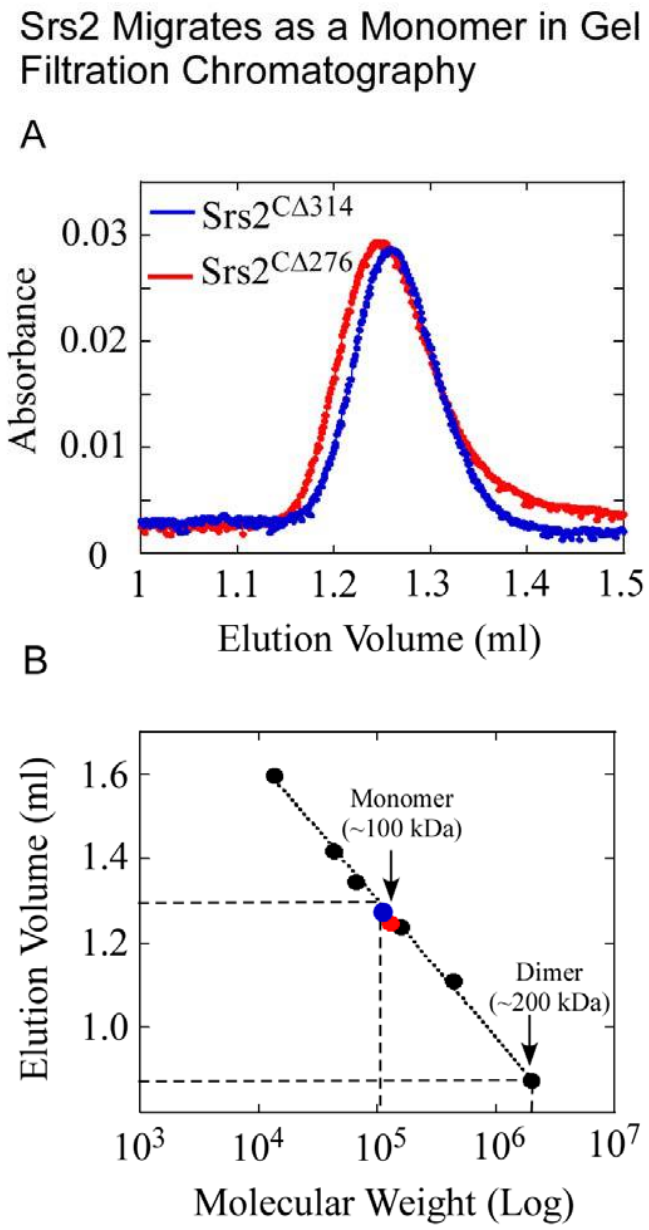

Figure S1. Srs2$^{C\Delta276}$ and Srs2$^{C\Delta314}$ are monodisperse in solution. (A) Elution profiles of Srs2$^{C\Delta276}$ (red) and Srs2$^{C\Delta314}$ (blue) on a size exclusion (S200) column. (B) A semilog plot of the elution volumes versus molecular weight (log) was constructed using a standard set of globular protein standards to determine the apparent molecular weight of the Srs2 proteins.

Molecular Cell, Vol. 35, No. 1 (July 10, 2009): pg. 105-115. DOI.

Figure S2

A Monomer of Srs2 is Bound on ssDNA During Translocation

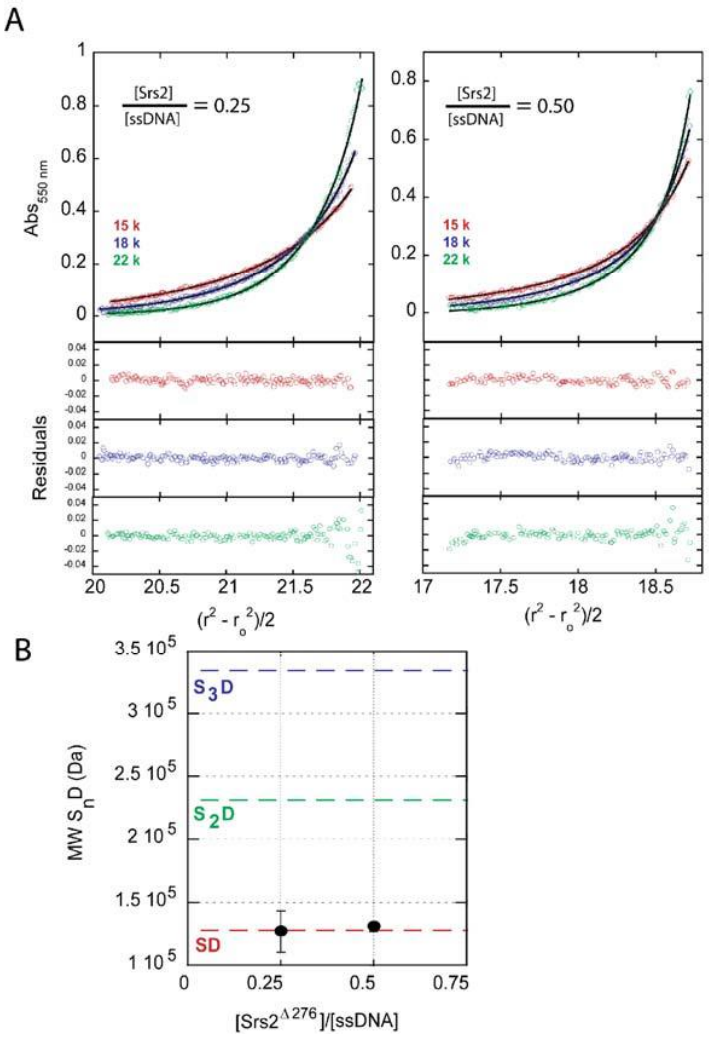

Figure S2. A $Srs2^{C\Delta276}$ monomer is bound per ssDNA under conditions of molar excess of ssDNA. Sedimentation equilibrium experiments were carried out in SF-buffer at 25°C using a dT_{79} nt ssDNA labeled with Cy3 at the 5'-end (5'-Cy3-dT_{79}). (A) Absorbance profiles are shown for experiments conducted with 2-fold and 4-fold molar excess of ssDNA over the protein concentration at 15,000; 18,000; and 22,000 rpm. The data were analyzed by equation (1) with n = 2, consistent with two species present in solution, free ssDNA and a Srs2:ssDNA complex. Smooth curves overlaying the data are simulations using the best-fit parameters from the global fit. (B) The values of the molar mass obtained from the fit for the Srs2:ssDNA complex are plotted as a function of the molar ratio of the total loading concentrations of Srs2 to ssDNA. The expected molar mass for 5'-Cy3-dT_{79} bound to one $Srs2^{\Delta276}$ monomer (SD), two $Srs2^{\Delta276}$ monomers (S_2D), or three $Srs2^{\Delta276}$ monomers (S_3D) are shown by dashed lines. Error bars represent 95% confidence limits (see supplemental methods).

Molecular Cell, Vol. 35, No. 1 (July 10, 2009): pg. 105-115. DOI.

Figure S3

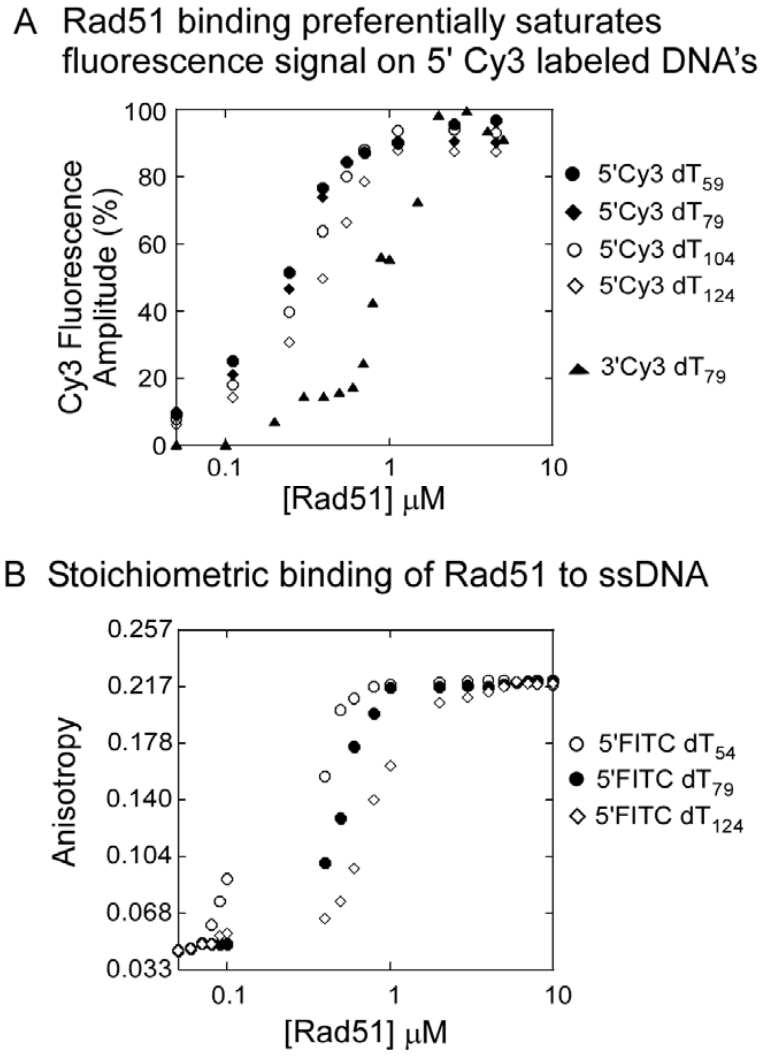

Figure S3. Assembly of Rad51 filaments on ssDNA (A) Kinetics of Rad51 binding to 5'Cy3 labeled dT oligonucleotides of varying lengths (dT_n = 59, 79, 104 and 124 nt) or a 3'Cy3 dT_{79} substrate. Increasing concentrations of Rad51 (0-10 μM) were rapidly mixed with 5'Cy3 dT79 ssDNA (40 nM) and ATP-Mg^{2+} (5 mM) using a stopped flow instrument. The total change in Cy3 fluorescence amplitude from each experiment is plotted as a function of Rad51 concentration. (B) The stoichiometry of Rad51 molecules bound to 5'FITC labeled dTn oligonucleotides (n = 54, 79 or 124) was measured using fluorescence anisotropy. Increasing concentrations of Rad51 (0 – 10 μM) were mixed with 5'FITC labeled dT79 oligonucleotide (40 nM) and the change in fluorescence anisotropy was measured.

Molecular Cell, Vol. 35, No. 1 (July 10, 2009): pg. 105-115. DOI.

Figure S4

A $Srs2^{C\Delta276}$ catalytically clears Rad51 filaments formed on a dT_{124} oligonucleotide

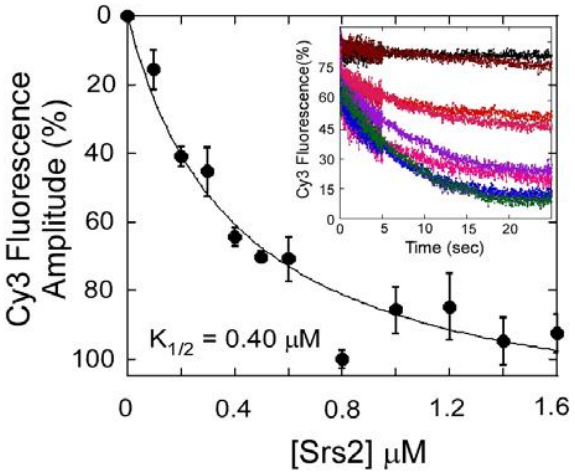

B $Srs2^{C\Delta276}$ catalytically clears Rad51 filaments formed on a dT_{79} oligonucleotide

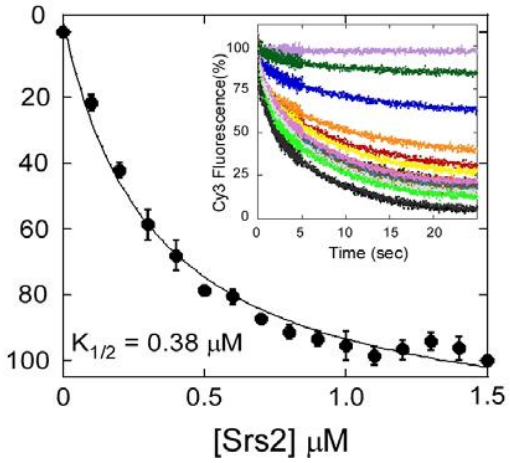

Figure S4. A) $Srs2^{C\Delta276}$ concentration dependence of Rad51 clearing on longer nucleoprotein filaments. Rad51 filaments were formed on a 5'Cy3 dT_{124} oligonucleotide (40 nM) with Rad51(4 μM) and ATP (5 mM), and filament clearing initiated by rapidly mixing with increasing concentrations of $Srs2^{C\Delta276}$ (0 – 3.2 μM, shown as insert). The relative change in fluorescence amplitude is plotted as a function of Srs2 concentration and yields a $K_{1/2}$ = 0.20 μM for Rad51 filament clearing by $Srs2^{C\Delta276}$ on long nucleoprotein filaments. The post-mixing concentrations are plotted in the graph. B) $Srs2^{C\Delta276}$ concentration dependence of Rad51 clearing on shorter (dT_{79}) nucleoprotein filaments (*cf* from Figure 3B).

Molecular Cell, Vol. 35, No. 1 (July 10, 2009): pg. 105-115. DOI.

Figure S5

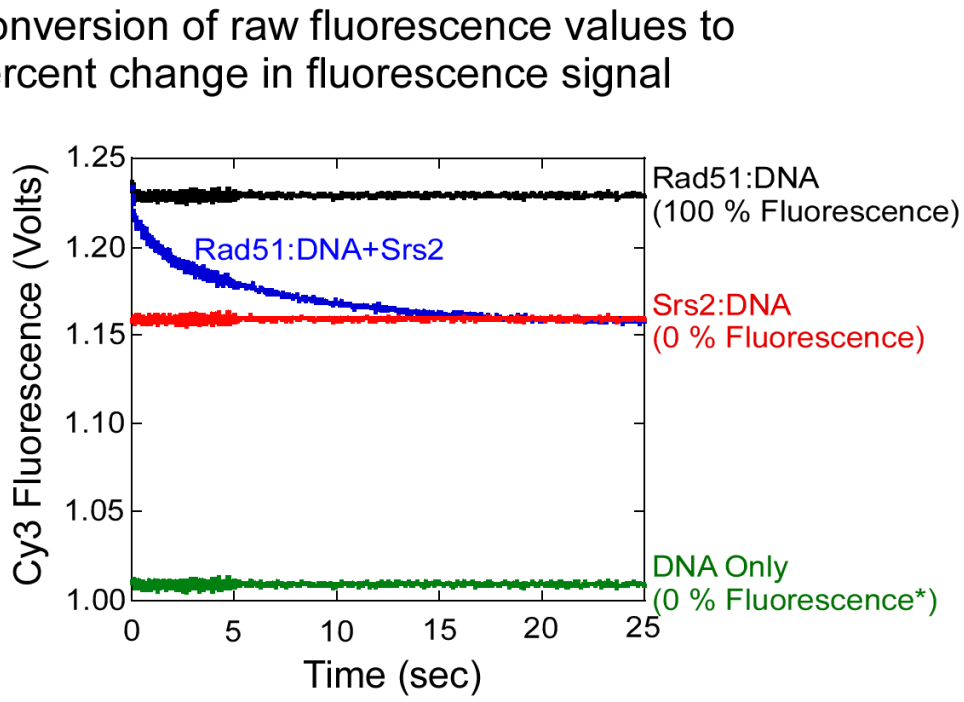

Figure S5. Control experiments used to calculate the percent change in fluorescence signal in stopped flow experiments. The fluorescence signal from a preformed Rad51:DNA complex (black trace) was used as the maximal fluorescence value (100 %). The signal from the preformed Srs2:DNA complex (red) was used as the signal for complete disassociation of Rad51 nucleoprotein filaments (0 %). The blue trace shows the disassembly of preformed Rad51filaments when Srs2 is added to the reaction. The basal level of fluorescence of the Cy3 labeled DNA used in our studies is shown in green, and this signal is used as the reference (0 %; marked by an asterisk) for the spontaneous Rad51 disassociation experiments described in Figure 2.

Molecular Cell, Vol. 35, No. 1 (July 10, 2009): pg. 105-115. DOI.